www.sciencemag.org/cgi/content/full/science.1235005/DC1

Supplementary Materials for

Dynamically Reshaping Signaling Networks to Program Cell Fate via Genetic Controllers

Kate E. Galloway, Elisa Franco, Christina D. Smolke*

*Corresponding author. E-mail: csmolke@stanford.edu

Published 11 July 2013 on *Science* Express
DOI: 10.1126/science.1235005

This PDF file includes

Materials and Methods

Plasmid and strain construction

Standard molecular biology cloning techniques were used to construct all plasmids (*53*). DNA synthesis was performed by Integrated DNA Technologies (Coralville, IA). All enzymes, including restriction enzymes and ligases, were obtained through New England Biolabs (Ipswich, MA). PCRs were performed with Expand High Fidelity PCR system (Roche, Indianapolis, IN) according to the manufacturer's instructions. Ligation products were electroporated with a GenePulser XCell (Bio-Rad, Hercules, CA) into an *E. coli* DH10B strain (Invitrogen, Carlsbad, CA), where cells harboring cloned plasmids were maintained in Luria-Bertani media containing 50 mg/ml ampicillin (EMD Chemicals). All cloned constructs were sequence verified by Laragen, Inc. (Santa Monica, CA). All confirmed plasmids were transformed into the appropriate yeast strains via standard lithium acetate procedure (*54*).

All reporter plasmids expressing GFP were constructed from pCS321 (URA selection; fig. S12A and table S4) (*24*). Yeast promoters *pADH1*, *pCYC1*, *pTEF1m7* (*pC*) (*55*), and *pFUS1* (*pFB*) (*56*) were PCR amplified from plasmid templates as specified and cloned into unique SacI (or NotI) and BamHI restrictions sites in pCS321 using promoter-specific primers (table S5).

Plasmids for galactose-titration of pathway regulators were constructed from pCS1128 (TRP selection), which harbors *pGAL1-yEGFP-CYCt* with an ON state RNA transducer control in the 3' UTR between AvrII and XhoI (fig. S12B and table S6). Yeast mating pathway genes (*STE4, STE50, STE11, STE7, FUS3, MSG5*) were cloned into this construct between AvrII and BamHI, replacing *yEGFP*, using gene-specific primers to amplify the desired fragments from

plasmid and genomic templates (table S5) (*20, 57*). Undesired restriction sites in the mating genes (e.g., XhoI in *FUS3* and *STE4*, AvrII in *STE7*) were removed by site-directed mutagenesis using QuikChange II Site-directed mutagenesis kit (Agilent, Santa Clara, CA), according to the manufacturer's instruction with appropriate primers (table S7).

The single-cassette negative and positive diverters (positive: *pC/FB-Ste4-SXtc*; negative: *pC/FB-Msg5-SXth*) were constructed by cloning *MSG5* and *STE4* into the GFP-expressing constructs with the appropriate promoters to replace *yEGFP* via AvrII and BamHI restriction sites as described above for the galactose-titration constructs. The RNA transducers (i.e., ribozyme devices) and appropriate controls (table S8) were PCR amplified from plasmid templates using the appropriate primers (table S9) subsequently inserted into the 3' UTR of these constructs via the unique restriction sites AvrII and XhoI, located immediately downstream of the gene stop codon as described previously (table S10 and S11) (*24*). The ON and OFF state controls for the RNA transducers correspond to the inactive and active ribozyme controls (representing the fully 'on' and 'off' gene expression states from the devices) as previously described (*24*). RNA transducers were previously constructed and characterized as described (*24, 35*) except for S3tc. S3tc was cloned into pCS1748 downstream of the reporter cassette (*pTEF1-GFP*) between AvrII and XhoI (*35*). To build pCS2450, S4tc was cloned into pCS1748 via AvrII and XhoI utilizing the primer Switch.NheI.FWD to insert a NheI site into the PCR insert. S1OFFth (with AvrII and XhoI 3' and 5' ends, respectively) was subsequently cloned into pCS2450 via NheI (compatible with AvrII sticky ends) and XhoI, ultimately removing the NheI site in the final construct pCS2451. S3tc was transformed into CSY3 and characterized as previously described (*35*).

The dual-cassette negative and positive diverters (positive feedback: *pFB-Ste4-SXtc*; resistance: *pC-Msg5-SXth*) were constructed by cloning the appropriate expression modules into the dual-cassette plasmid pCS2094 (*35*) (URA selection; fig. S13A and table S12). The positive feedback module (*pFB-Ste4-S2tc*) was amplified via PCR from the single-cassette positive diverter plasmid with primers pFUS1.ClaI.pCS2094.FWD (5'-CCAATCTCAGAGGCTGAGTC TC) and Switch3'.XhoI.pCS2094.REV (5'-AAAACTCGAGTTTTTATTTTTCTTTTTGCTGTT TCG) and cloned into the unique ClaI and XhoI restriction sites in pCS2094 to construct pCS2515 (fig. S13B). Tetracyline-responsive RNA transducers and appropriate controls (table S8) were inserted into the 3' UTR of *STE4* via the unique restriction sites AvrII and XhoI, located immediately downstream of the *STE4* stop codon as described previously (*24*). Resistance expression modules (*pC-Msg5-SXth*) were PCR amplified from the single-cassette negative diverter plasmids (table S10) with primers pTEF7.FWD (5'-AAGAGCTCATAGCTTC AAAATGTCTCTACTCCTTTTT) and CYC1t.NotI.REV (5'-AAAAGCGGCCGCTATATTAC CCTGTTATCC) and cloned into the unique SacI and NotI restriction sites in constructs harboring the positive feedback modules (fig. S13C and table S12).

A second dual-cassette plasmid (TRP selection) was constructed for the negative feedback and booster modules (negative feedback: *pFB-Msg5-SXth*; booster: *pC-Ste4-SXtc*). A dual-expression plasmid, pCS2521, harboring the positive feedback module with OFF state control and a second expression cassette bearing *pTEF1-mCherry-CYC1t* was digested with SacI and KpnI. The dual-expression cassette fragment was gel extracted and inserted via these same unique restriction sites into pCS1128 (TRP selection) to construct pCS2540. Negative feedback modules (*pFB-Msg5-SXth*) were PCR amplified from the single-cassette negative feedback diverter plasmids (table S10) using primers Msg5.K2.FWD (5'-AAAGGATCCAATTAATAGT

GCACATGCAATTTCAC) and Switch3'.XhoI.pCS2094.REV and cloned into the unique BamHI and XhoI restriction sites in pCS2540 (fig. S14A). Booster expression modules (*pC-Ste4-SXtc*) were PCR amplified from the single-cassette booster diverter plasmids (table S11) with primers pTEF7.FWD and CYC1t.NotI.REV and cloned into the unique SacI and NotI restriction sites in constructs harboring the negative feedback modules (fig. S14B and table S13). Additionally, single-cassette booster diverters (*pC-Ste4-SXtc*) were cloned into the pCS1128 backbone (TRP selection) via SacI and KpnI (table S14) for pairing with pCS2094-based backbones (URA selection).

The galactose-titration studies were performed in yeast strains that have the galactose transporter *GAL2* knocked out. The *pFUS1-yEGFP3-CYC1t* cassette from pCS1124 was cloned into pCS1391, a loxP integrating vector (*58*), via the unique SacI and KpnI restriction sites to construct pCS2292 (table S15). The *pFUS1-yEGFP3-CYC1t* expression cassette from pCS2292 was subsequently chromosomally integrated into yeast strain CSY364 (EY1119; W303a Δsst1 Δkss1::HIS3) (*59*) via homologous recombination to construct yeast strain CSY532 (W303a Δsst1 Δkss1::HIS3 gal2::FUS1p-yEGFP3-loxP-KanR-loxP) (table S16). Briefly, the *pFUS1-yEGFP3-loxP-KanR-loxP* cassette was PCR amplified from pCS2292 using forward and reverse primers harboring 60 nts of homology to the *GAL2* locus (table S17). Yeast strain CSY364 was transformed with 12 μg of gel purified PCR product and plated on G418 plates to select for the *GAL2* knock-out, integrated *pFUS1-GFP* reporter strain CSY532. The characterization strain for the molecular network diverters (CSY840, W303a Δsst1 Δkss1::HIS3 trp1::FUS1p-yEGFP3-loxP-KanR-loxP) was constructed as described for CSY532, except primers specific to the *TRP1* locus were used for integrating the reporter cassette (table S17).

Measuring promoter and RNA transducer activities

To characterize promoter activities, promoter-GFP fusions were constructed as described (table S4) and transformed into CSY364. Cells were inoculated into the appropriate dropout media, grown overnight at 30°C, and back diluted into fresh media. For *pFB*, GFP values were determined in the absence (pFB-) and presence (pFB+) of saturating α factor 3 h following stimulation. Following 6 h of growth post-back dilution, GFP fluorescence levels from the *pX-yEGFP3* reporter were evaluated via flow cytometry using a Cell Lab Quanta SC flow cytometer (Beckman Coulter, Fullerton, CA). GFP was exited from a 488 nm laser and emission was measured from 520/40 nm bandpass filter with a PMT setting of 5.0. Cells were gated for viability based on side scatter and EV. For each sample, the GFP values of 10,000 viable cells were measured. Cells were then gated for GFP levels above background. Flow cytometry data was analyzed using the FlowJo v.10 (Tree Star, Inc.) software package. Normalized GFP expression is reported as the geometric mean GFP value from cells harboring the specified construct normalized to that of the control (cells harboring the *pC* construct). RNA transducers were characterized as previously described (*35*). Briefly, transducers regulating the *pTEF1-yEGFP3* reporter were characterized for GFP fluorescence on a Quanta flow cytometer as described above. Transducer activity was determined as the geometric mean of the GFP fluorescence based for population gate above background using FlowJo v.10 (Tree Star, Inc.) software package, and normalized to the geometric mean of the GFP fluorescence of the ON positive control (sTRSV Ctrl).

Calculating relative regulator expression

For non-feedback constructs, relative regulator (Ste4/Msg5) expression was calculated from measured values of the relative promoter activities (Fig. 2C) and the various RNA transducer activities (Fig. 2, D and E). Briefly, for each promoter-transducer pairing the calculated expression amount was determined as the relative GFP expression (from the promoter) multiplied by the relative GFP expression (from the transducer at the appropriate signal molecule concentration). Relative regulator expression values were determined as the calculated expression amount for the indicated construct normalized to that of a construct with the pairing of the *pC* promoter and ON RNA transducer control. For the positive feedback constructs (*pFB-Ste4-SX*), predicted expression of Ste4 was calculated using the measured transducer activity and the *pFB* promoter activity in the absence of pheromone to simulate the initial (t=0) Ste4 expression from the system. For the negative feedback constructs (*pFB-Msg5-SX*), the value of the relative promoter activity was determined from relative GFP expression levels (or normalized pathway activity values) in reporter strains (*pFUS1-GFP*) harboring Msg5 constructs under feedback control (*pFB*) paired with the various transducers (*SX*).

Evaluating selection of mating resistance population

The selection of a mating resistant population over time from cell populations undergoing high levels of growth arrest was evaluated in cells expressing Ste4 from the galactose-inducible promoter (*pGAL-STE4-ON*) and blank plasmid control in yeast strain CSY532. Cells were inoculated into the appropriate dropout media, grown overnight at 30°C, and back diluted into fresh media to an OD_{600} of <0.1. Briefly, cells were grown for 48 h in the presence of pheromone (100 nM). Cells were back diluted into fresh media at 0, 6, 18, 30 and 42 h maintaining the

pheromone concentration. Mean fluorescence values for GFP were measured by flow cytometry as described previously at 0, 6, 24, 30, and 48 h. For measurement time points corresponding to back-dilution time points, cells were measured prior to back dilution. Values represent the mean of at least three biological replicates and error bars represent standard deviation**.** Halo assays were performed as described previously at the indicated galactose concentrations after 48 h of growth. Representative images are presented from experiments performed in triplicate.

Additionally, cells expressing Ste4 from the galactose-inducible promoter (*pGAL-STE4-ON*) were grown in the presence or absence of galactose (0, 2%). Cells were back diluted into fresh media at 0, 12, 24, 36 and 48 h maintaining the galactose concentration. Mean fluorescence values for GFP were measured by flow cytometry as described previously at time points 0, 6, 12, 30, 36, and 54 h. For measurement time points corresponding to back-dilution time points, cells were measured prior to back dilution. Values represent the mean of at least three biological replicates and error bars represent standard deviation**.** Halo assays were performed as described previously at the indicated galactose concentrations after 54 h of growth. Representative images are presented from experiments performed in triplicate.

Determining resolution and variation in positive diverter networks.

Resolution was determined by setting a gate at the lowest ~5% of the triggered population. The percentage of cells in the population falling above this gate were determined for both triggered and untriggered cells (untriggered/triggered: 0/1 mM tetracycline). Resolution is reported as the ratio of the % of triggered cells that fell above this gate to the % of total cells (% triggered and % untriggered cells) that fell above this gate. The coefficient of variation (CV) was determined for viable cells above background fluorescence using the CV function in FlowJo v.10

(Tree Star, Inc.) software package. Values were normalized to the CV cells harboring the blank plasmid control stimulated with saturating pheromone (100 nM). Values represent mean of at least three biological replicates and error bars represent standard deviation**.**

Measuring mating efficiencies

Quantitative mating assays were performed as previously described (*60*). Briefly, experimental yeast strains (*MATa*) harboring the indicated constructs to be tested for mating efficiency were grown to an OD_{600} of 0.4-0.8 and back diluted into the appropriate media containing the indicated concentration of signal molecule (theophylline or tetracycline). Following 3 h of growth post-back dilution, 1x 10^6 cells of the experimental strain were mixed with 1x10^7 cells of the MAYA12 (*MATα –lys1*) tester strain (*60*). The mixture of cells was collected on a 0.45 µm pore, 25 mm nitrocellulose filter disc and placed on YPD plates for 5 h at 30^{o}C. Cells were resuspended by vortexing the disc in 1 mL of yeast nitrogen base (YNB). The resuspended cell mixture was serially diluted 1:10 in YNB to make dilutions 10^{-1}, 10^{-2}, 10^{-3}, and 10^{-4}. To titer diploids, 200 µl of the 10^{-2} dilution was plated on total dropout plates. To titer the experimental strain, 200 µl of the 10^{-3} and 10^{-4} dilutions were plated on –LYS plates. Mating efficiency was calculated as the number of diploids normalized by the number of colonies from the –LYS plates (experimental strain and diploids). Data represents mean values from three or more independent replicates. Error bars represent the standard deviation of at least three replicates. P-values were determined using a two-tailed t-test of the compared data sets.

Supporting Text

Text S1: The selection of a mating-resistant population over time from cells programmed for high levels of growth arrest

Pathway activity was examined as a function of the calculated Ste4 expression to identify the threshold level at which cell fate diverges. The data shows a steady increase in pathway activity with increasing relative Ste4 expression up to a threshold value followed by a sharp drop (fig. S3A). The drop in pathway activity coincides with the divergence of fate observed in the halo assays. Only cells conditionally induced to higher Ste4 expression over the course of the assay exhibit high pathway activity, while cells programmed for invariantly high Ste4 expression exhibit low pathway activity, suggesting that over longer time periods high Ste4 expression may select for cells with inactive pathways. For example, despite being programmed for constitutive arrest the ON state control for Ste4 expression under the feedback architecture (*pFB-Ste4-ON*) exhibited low pathway activity and significant growth across the entire plate in halo assays indicating insensitivity to pheromone (Fig. 3A). These data suggest that over longer time periods high Ste4 expression may select for mating-resistant cells. Alternately, cells may escape persistent cell cycle arrest induced via high Ste4 expression via mutations inhibiting the expression of Ste4 or even via plasmid loss. For example, the ON state control for constitutive Ste4 expression (fig. S4 and S5A) demonstrates extra-halo growth at a reduced cell density indicating that a small fraction of the plated cells grow and respond to pheromone. Cells may utilize a combination of strategies to counteract constitutive cell-cycle arrest leading to diverse phenotypes that vary both across and within constructs and cultures representing a mix of selective pressures and hysteresis (fig. S5B).

While plasmid loss and/or mutation may account for the development of a population of cells displaying the wild-type phenotype in cells programmed for high Ste4 expression, these factors are insufficient to account for the uniform growth across the plate observed in halo assays (Fig. 3A). We postulated that strong Ste4 overexpression places selective pressure against cells with highly active pathways via growth arrest, such that over time the population is dominated by cells resistant to pathway activation and subsequent growth arrest. Consequently, cells harboring programs with constitutively high Ste4 expression display a low fluorescence profile from the *pFUS1-GFP* reporter and exhibit growth within the expected halo region indicating resistance to pheromone-induced cell cycle arrest. To test this hypothesis, we monitored the growth arrest behavior and GFP profile of cells harboring Ste4 galactose titration plasmid (*pGAL1-Ste4-ON*) or a blank plasmid (pCS1071). Cells were stimulated either via saturating pheromone for 48 h (fig. S3, B and C) or grown in the presence of galactose for 54 h (fig. S3, D and E). Following an initial increase in pathway activity, the activity of stimulated cells dropped to unstimulated levels (fig. S3, B and D). Cells persistently activated with pheromone or high Ste4 expression failed to form the characteristic halo indicating pheromone fails to induce cell cycle arrest in these cells (fig. S3, C and E). Cells naïve to galactose and pheromone stimulation (i.e., without previous exposure to either pheromone or galactose) maintained their responsiveness to both pheromone and galactose. Taken together the data confirm that persistent stimulation results in a cell population resistant to mating pathway activation. These results highlight the utility of genetic programs that run quiescently until activated for applications in which the program necessarily modulates cellular processes that place selection pressure on the population, such as growth rate and/or viability.

Supplementary Figures

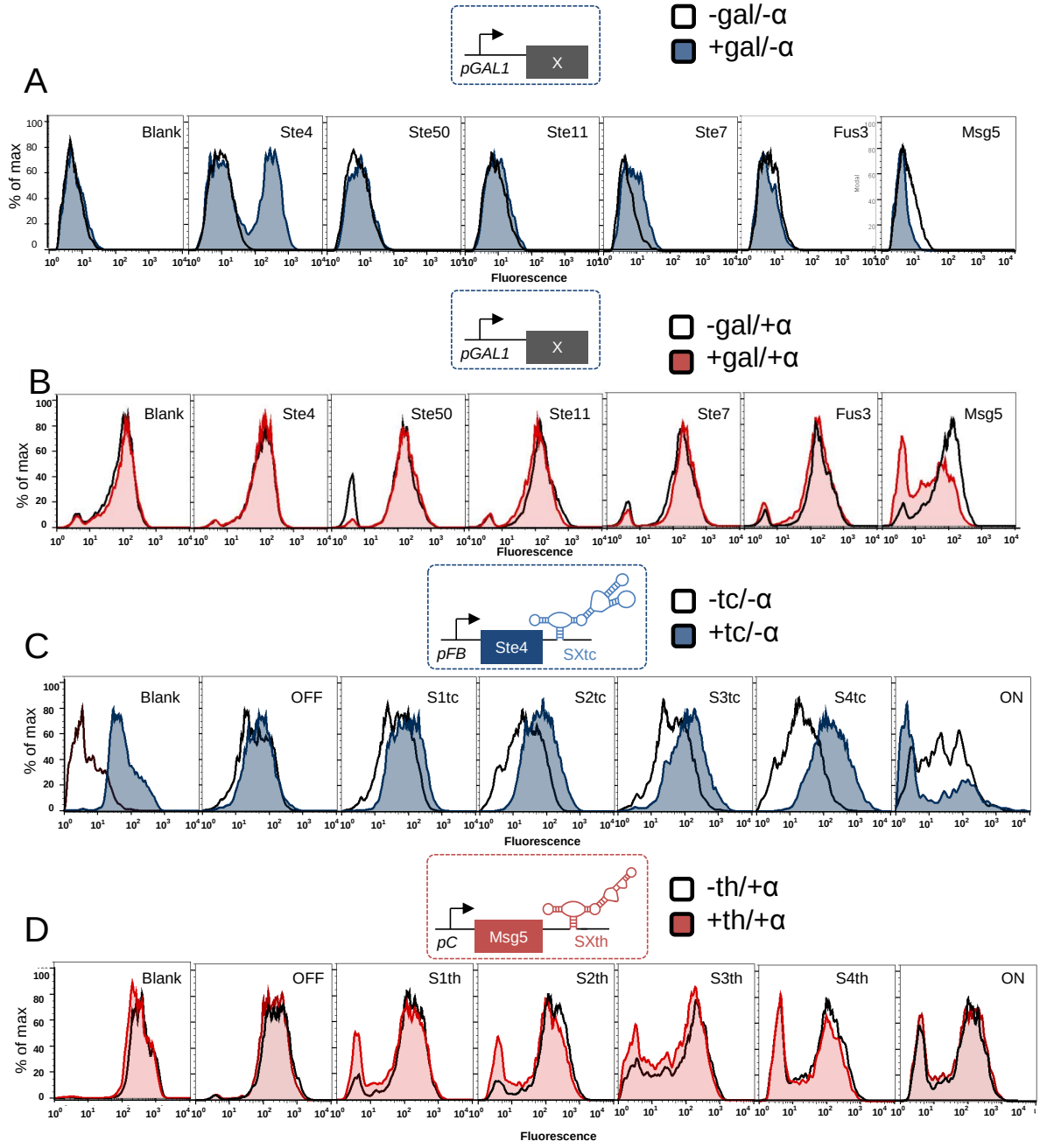

Figure S1. Raw flow cytometry histograms for pathway component sensitivity analysis and single molecular network diverters

(A, B) Flow cytometry histograms for cells harboring the indicated pathway genes overexpressed from *pGAL1* in the presence (+gal) or absence (-gal) of 1% galactose. Pathway activation is

measured in the absence of 100 nM pheromone (A, -α) and pathway attenuation is measured in the presence of 100 nM pheromone (B, +α). (C) Flow cytometry histograms for cells harboring the indicated positive feedback diverters with various transducers in the absence (-tc) or presence (+tc) of 1 mM tetracycline and in the absence of pheromone (-α). (D) Flow cytometry histograms for cells harboring the indicated resistance diverters with various transducers in the absence (-th) or presence (+th) of 5 mM theophylline and in the presence of 100 nM pheromone (+α). The data suggest that while the population-level pathway activity response to changes in Msg5 is graded, individual cells respond in a more "all-or-none" manner. Further, the variation in pathway activity may be magnified by the presence of external antagonism (i.e., saturating pheromone), cell-to-cell variation in Msg5 expression, and the potency of Msg5 as a regulator.

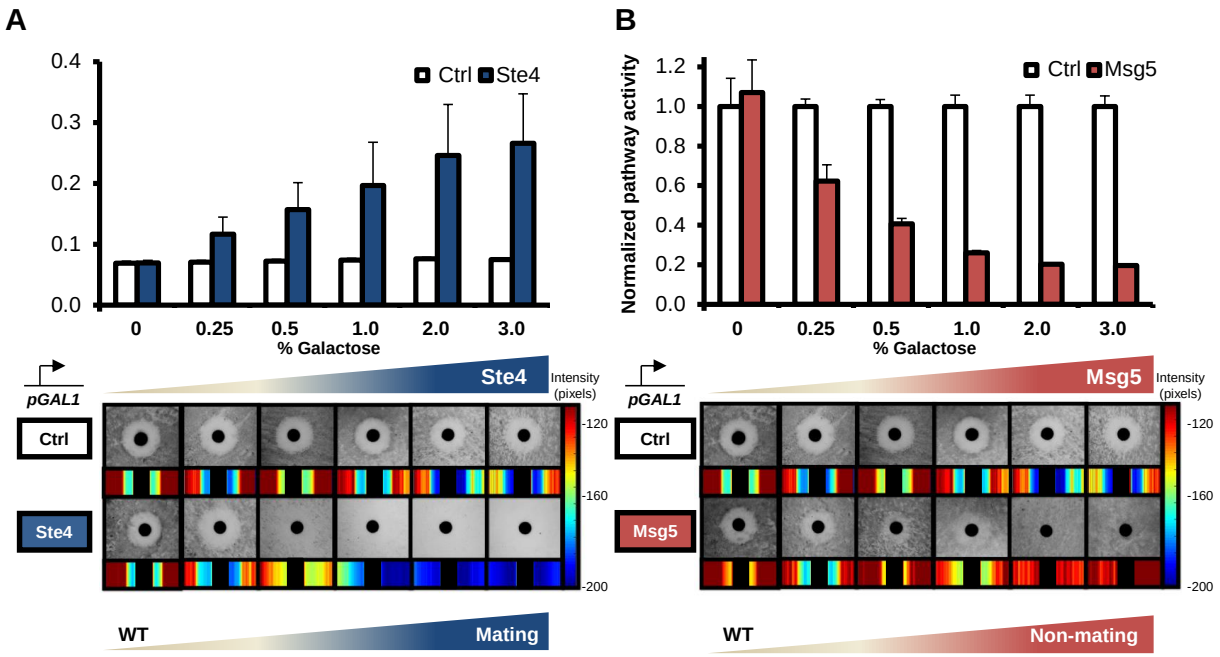

Figure S2. Titratable regulators of pathway activity in the yeast mating pathway route to alternate fates

(A) In the absence of pheromone, Ste4 overexpression increases pathway activity in a galactose-dependent manner, indicating it is a positive regulator. Overexpression of Ste4 routes cells to the mating fate characterized by pheromone-independent cell cycle arrest in halo assays. (B) Msg5 overexpression reduces pathway activity in pheromone stimulated cells, indicating it is a negative regulator. Overexpression of Msg5 routes cells to the non-mating fate characterized by reduced halo formation. Pathway activity is measured via a *pFUS1-GFP* reporter. Cells were cultured in 0, 0.25, 0.5, 1, 2, or 3% galactose for 6 h after back dilution prior to measurement on a flow cytometer. To characterize Msg5 (B), cells were stimulated with saturating pheromone 3 h post-back dilution. To identify activating regulators, normalized pathway activity is reported as the geometric mean GFP value from cells harboring the specified construct in the absence of pheromone at the indicated galactose concentration normalized to that of the control (cells

harboring a blank plasmid in the presence of saturating pheromone at the corresponding galactose concentration). To identify attenuating regulators, normalized pathway activity from attenuating constructs is reported as described above, except cells are assayed in the presence of saturating pheromone.

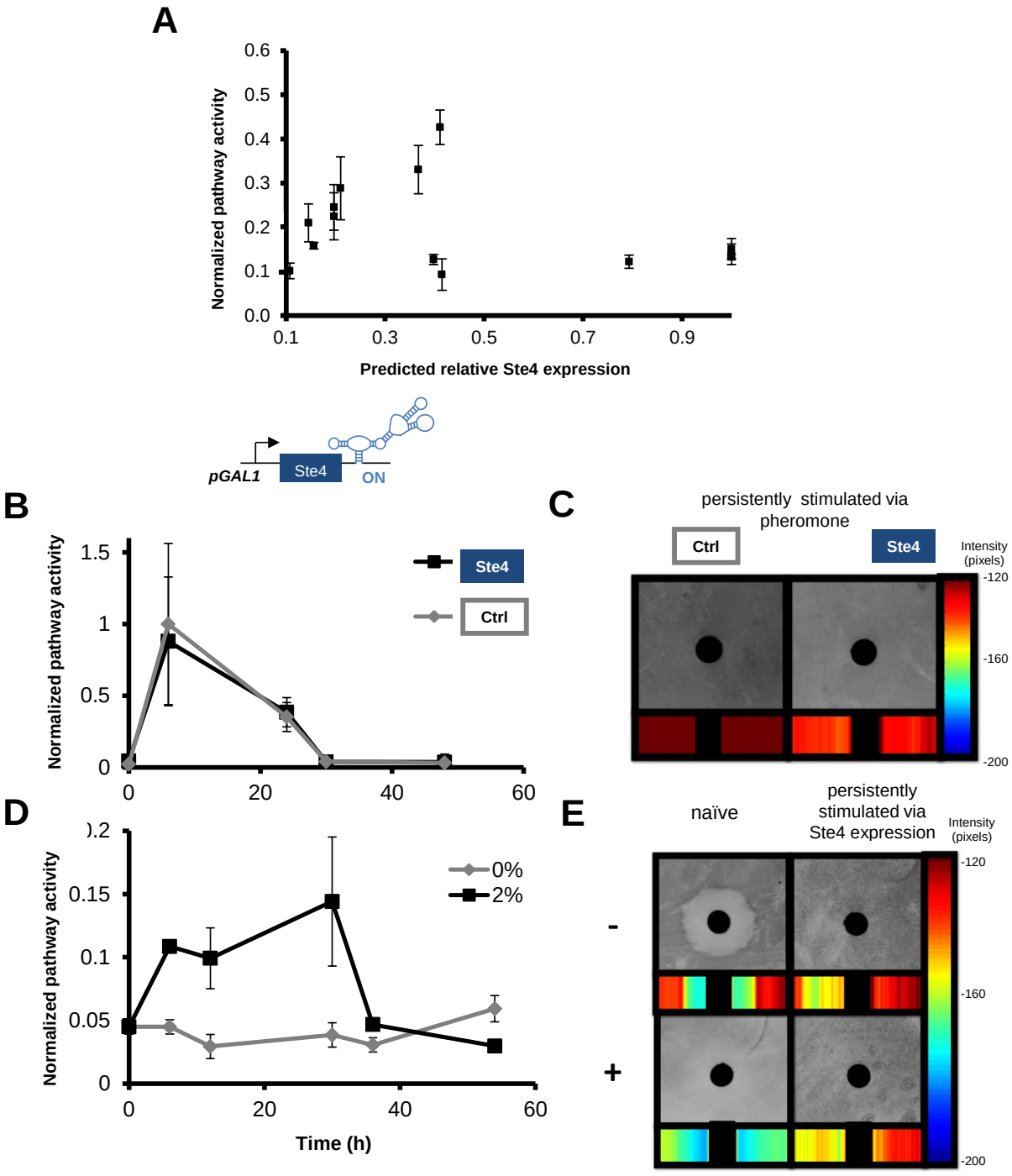

Figure S3. Persistent pathway activation results in the selection of mating-resistant cells

(A) Pathway activity increased with increasing Ste4 expression up to a threshold point. Above this threshold, pathway activity drops, indicating that strong Ste4 overexpression placed selective

pressure against cells through growth arrest such that cells resistant to pathway activation dominated the population over time. (B) Over time persistent stimulation with saturating pheromone results in a cell population dominated by cells unresponsive to pheromone. Cells harboring the construct *pGAL1-Ste4-ON* or a blank plasmid control were grown over 48 h in the presence of saturating pheromone. To maintain pheromone concentration and logarithmic growing conditions, cells were back diluted into fresh media every 12 h. Normalized pathway activity is reported as the geometric mean GFP value from cells harboring the specified construct at the indicated galactose concentration normalized to that of the control (cells harboring a blank plasmid in the presence of saturating pheromone in 0% galactose). (C) Halo assays indicate that over time persistent pheromone stimulation leads to a population dominated by cells resistant to pheromone-induced cell cycle arrest. Following 48 h growth in the presence of pheromone, halo assays were performed as described previously. (D) Over time high expression of Ste4 via the galactose-inducible system selects for cells resistant to Ste4-mediated pathway activation. Cells harboring the construct *pGAL1-Ste4-ON* were grown over 48 h in the presence or absence of galactose (0, 2%). To maintain galactose concentration and logarithmic growing conditions, cells were back diluted into fresh media every 12 h. (E) Halo assays indicate that over time persistent stimulation via Ste4 overexpression leads to a population dominated by cells resistant to pheromone-induced cell cycle arrest. Cells grown in the presence of galactose for 54 h show reduced responsiveness to galactose in halo assays with only slight decrease in density from 0% (-) to 2% (+) galactose. Cells grown for 54 h in the absence of galactose maintain responsiveness to both pheromone and galactose. Following 54 h growth in the presence of pheromone, halo assays were performed as described previously.

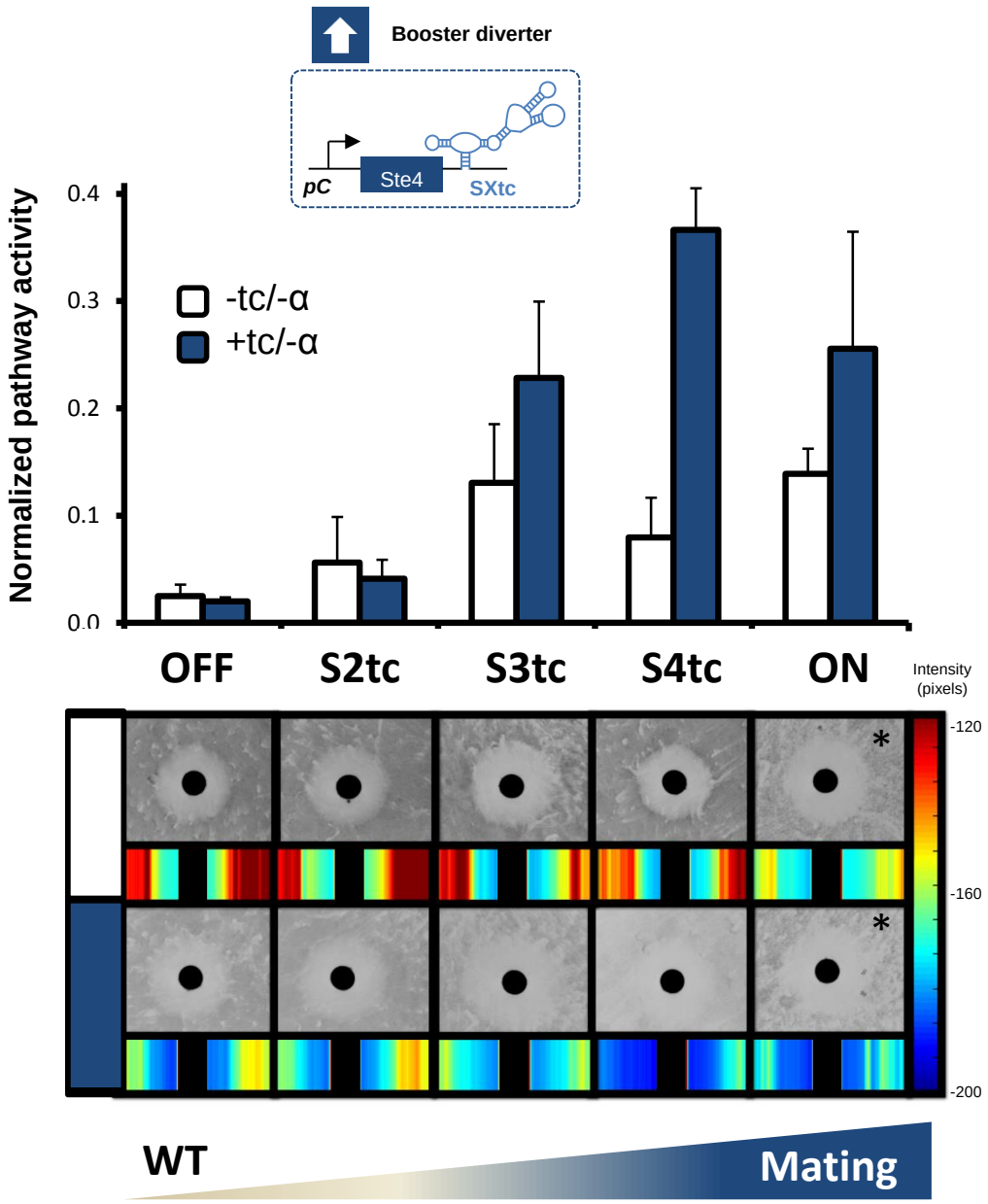

Figure S4. Positive diverters without feedback exhibit weak routing to the mating fate

A positive diverter without feedback, or booster diverter, (*pC-Ste4-S4tc*) exhibits wild-type fate in the absence of tetracycline and weak routing to the mating fate in response to tetracycline (-/+tc: 0/1 mM tetracycline; -α: 0 nM α mating factor). Asterisk: The ON state control shows significant growth in the presence and absence of tetracycline indicating that cells harboring this diverter have escaped the programmed growth arrest expected due to high Ste4 expression (SOM

text S1). Normalized pathway activity from activating constructs is reported as the geometric mean GFP value from cells harboring the specified construct in the absence of pheromone at the indicated signal concentration normalized to that of the control (cells harboring a blank plasmid in the presence of saturating pheromone).

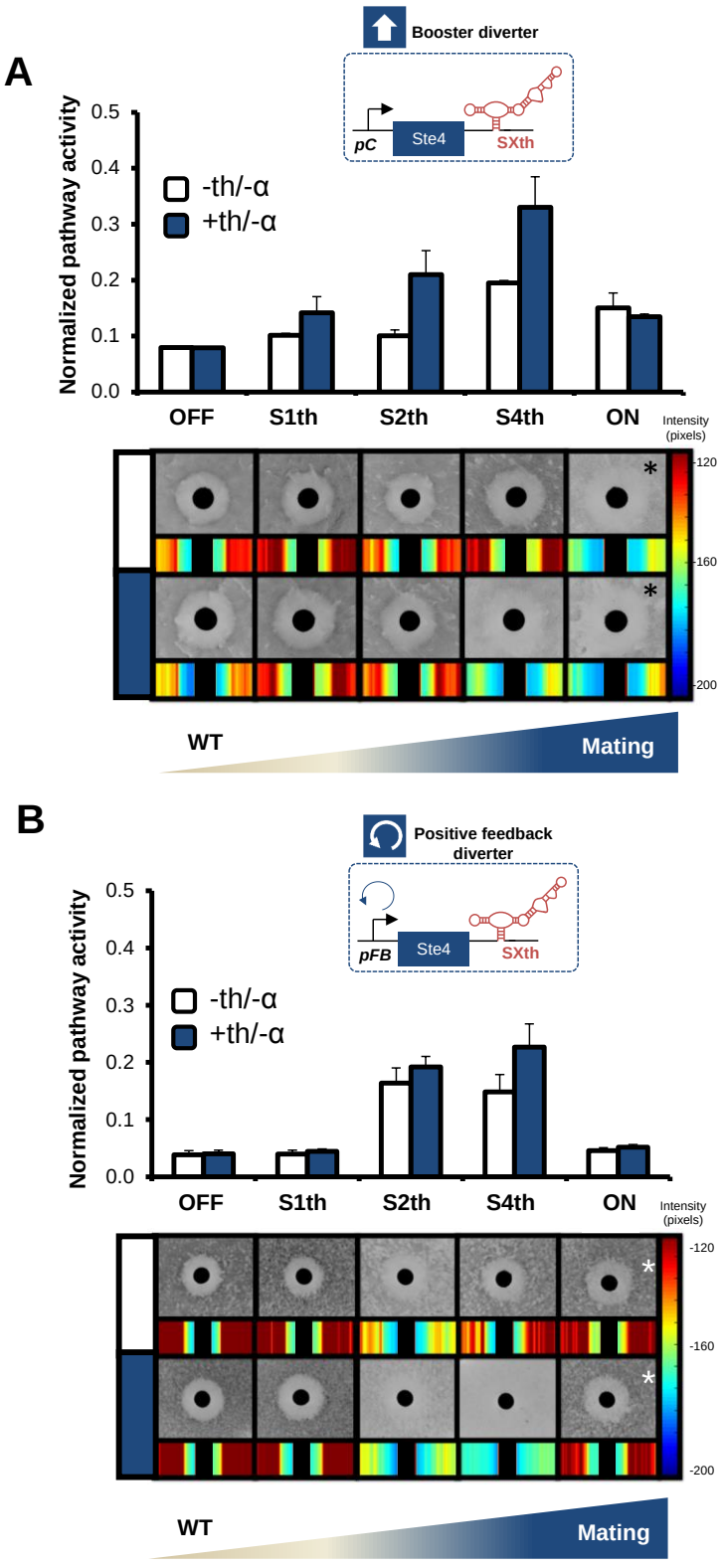

Figure S5. Network diverters can be programmed to respond to different environmental signals through the RNA transducer component

(A) The positive diverter without feedback, or booster diverter, is modified to respond to a different environmental signal by replacing the tetracycline-responsive RNA transducer with a theophylline-responsive RNA transducer. The theophylline-responsive booster diverters exhibit increased pathway activity in response to theophylline. The booster diverter *pC-Ste4-S4th* exhibits wild-type fate in the absence of theophylline and weak routing to the mating fate in the presence of theophylline (-/+th: 0/5 mM theophylline; -α: 0 nM α mating factor). Normalized pathway activity from activating constructs is reported as the geometric mean GFP value from cells harboring the specified construct in the absence of pheromone at the indicated signal concentration normalized to that of the control (cells harboring a blank plasmid in the presence of saturating pheromone). (B) The positive feedback diverter is modified to respond to a different environmental signal by replacing the tetracycline-responsive RNA transducer with a theophylline-responsive RNA transducer. The theophylline-responsive positive feedback diverters exhibit slightly increased pathway activity in response to theophylline. The positive feedback diverter *pFB-Ste4-S4th* exhibits wild-type fate in the absence of theophylline and robust routing to the mating fate in the presence of theophylline. Asterisk: The ON state control shows significant growth in the presence and absence of theophylline indicating that cells harboring this diverter have escaped the programmed growth arrest due to high Ste4 expression (SOM text S1).

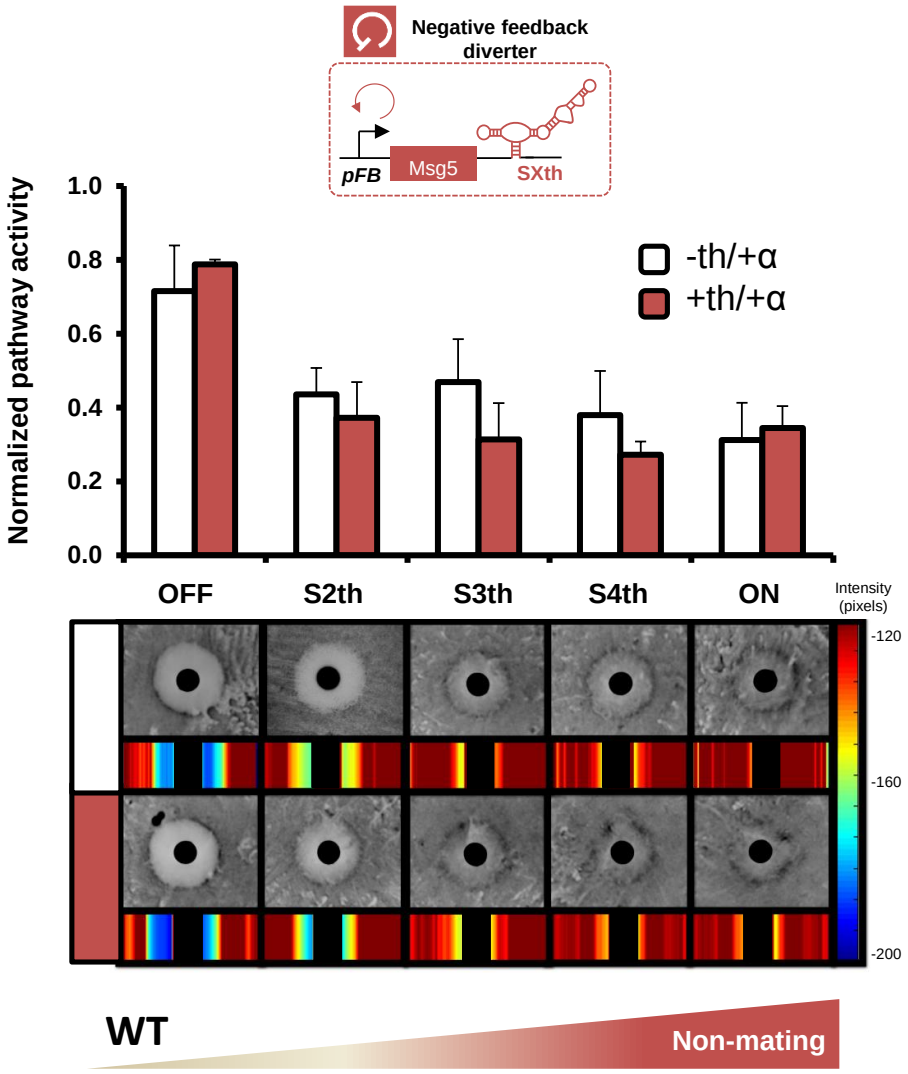

Figure S6. Negative feedback diverters result in reduced pathway activity and a weak response to the trigger molecule

No single negative feedback diverter (*pFB-Msg5-SXth*) exhibits robust routing between the wild-type and non-mating fates (-/+th: 0/5 mM theophylline; +α: 100 nM α mating factor). Normalized pathway activity from attenuating constructs is reported as the geometric mean GFP value from cells harboring the specified construct in the presence of saturating pheromone at the indicated signal concentration normalized to that of the control (cells harboring a blank plasmid in the presence of saturating pheromone).

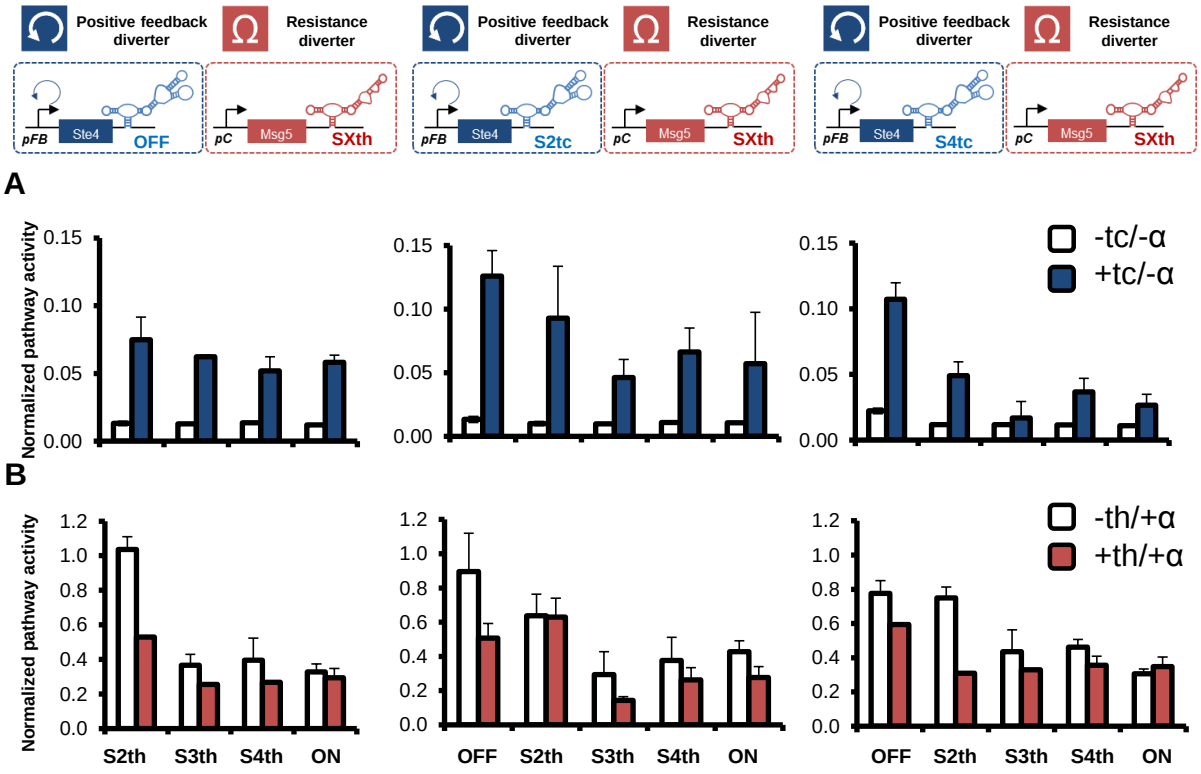

Figure S7. Dual-router architectures based on integrating the positive feedback and resistance diverters fail to achieve dual fate routing

(A) Combining positive feedback diverters (left: *pFB-Ste4-OFF*; center: *pFB-Ste4-S2tc*; right: *pFB-Ste4-S4tc*) with negative diverters without feedback, or resistance diverters, of varying strength (*pC-Msg5-SXtc*) inhibits pathway activation (-/+tc: 0/1 mM tetracycline; -α: 0 nM α mating factor). Normalized pathway activity from activating constructs is reported as the geometric mean GFP value from cells harboring the specified construct in the absence of pheromone at the indicated signal concentration normalized to that of the control (cells harboring a blank plasmid in the presence of saturating pheromone). (B) Pathway attenuation increases with increasing resistance strength (-/+th: 0/5 mM theophylline; +α: 100 nM α mating factor). Normalized pathway activity from attenuating constructs is reported as the geometric mean GFP value from cells harboring the specified construct in the presence of saturating pheromone at the

indicated signal concentration normalized to that of the control (cells harboring a blank plasmid in the presence of saturating pheromone).

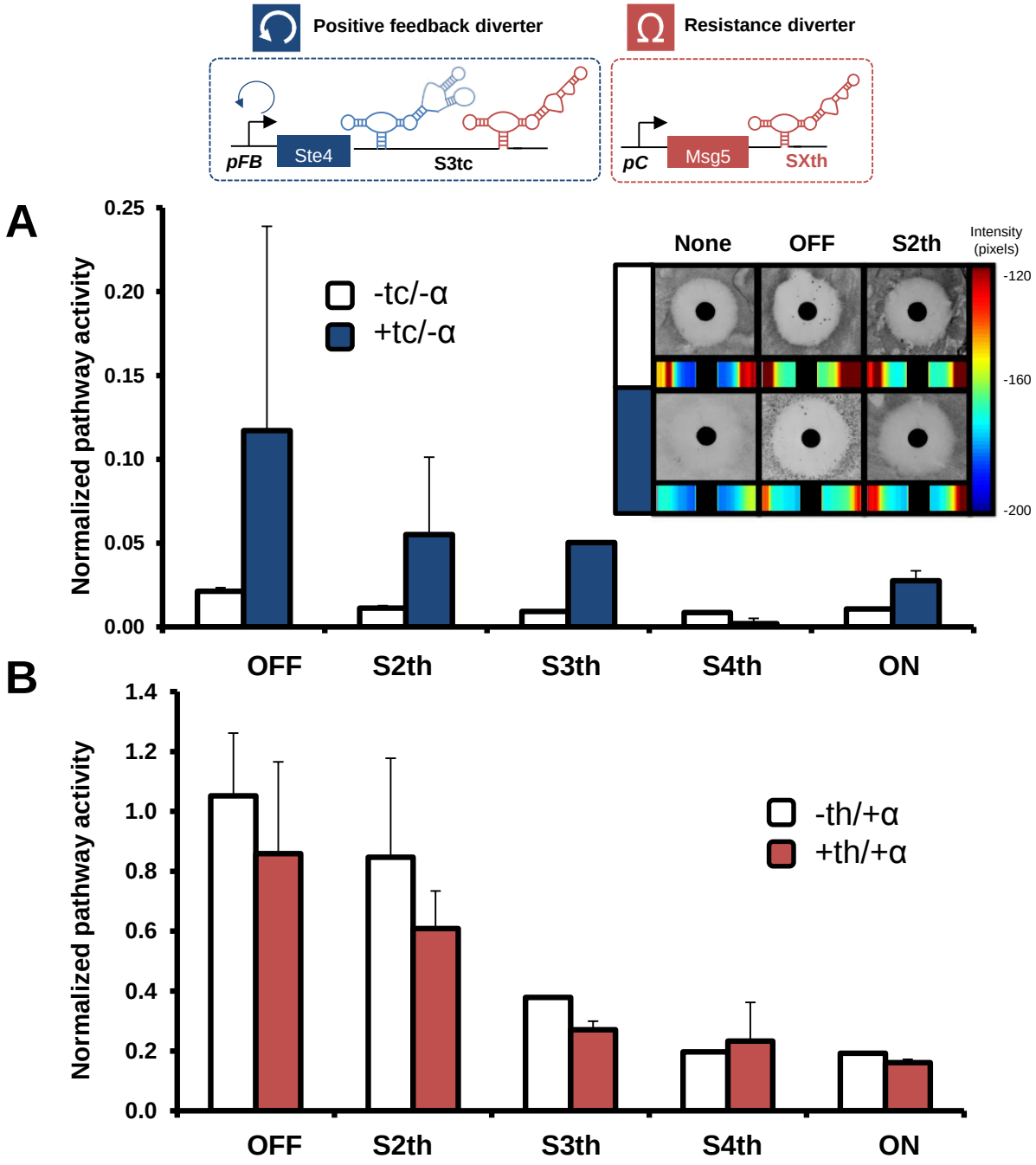

Figure S8. A dual-router architecture based on integrating the improved positive feedback diverter with reduced antagonism with resistance diverters fails to achieve dual fate routing

(A) Combining the positive feedback diverter designed for reduced antagonism (*pFUS1-Ste4-S3tc*) with negative diverters without feedback, or resistance diverters, of varying strength (*pC-Msg5-SXth*) inhibits pathway activation (-/+tc: 0/1 mM tetracycline). Inset shows that cells harboring the positive feedback diverter (*pFUS1-Ste4-S3tc*) paired with the resistance diverters (OFF, S2th) fail to route to the mating fate. In contrast, cells harboring the positive feedback diverter without a resistance cassette (none) route to the mating fate in response to 1 mM tetracycline. Normalized pathway activity from activating constructs is reported as the geometric mean GFP value from cells harboring the specified construct in the absence of pheromone at the indicated signal concentration normalized to that of the control (cells harboring a blank plasmid in the presence of saturating pheromone). (B) Pathway attenuation from resistance diverters of varying strength (*pC-Msg5-SXth*) paired with the positive feedback diverter that reduces positive feedback strength in response to theophylline (*pFUS1-Ste4-S3tc*) is similar to configurations with lower strength positive feedback modules (fig. S10; -/+th: 0/5 mM theophylline; +α: 100 nM α mating factor). Normalized pathway activity from attenuating constructs is reported as the geometric mean GFP value from cells harboring the specified construct in the presence of saturating pheromone at the indicated signal concentration normalized to that of the control (cells harboring a blank plasmid in the presence of saturating pheromone).

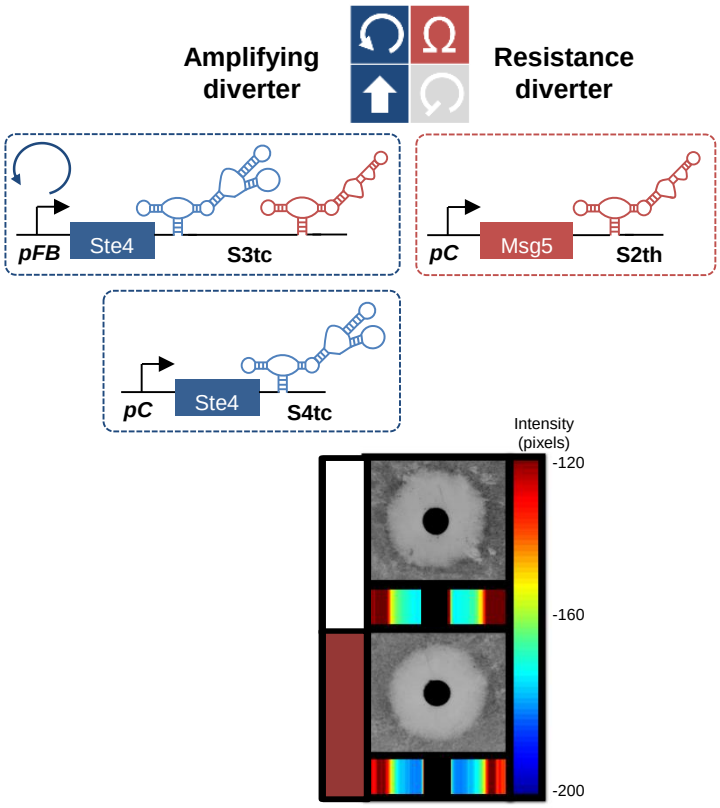

Figure S9. A dual-router architecture based on integrating the amplifying diverter with the resistance diverter fails to route cells to the non-mating fate

Cells harboring the amplifying diverter (positive feedback module: *pFB-Ste4-S3tc;* booster module: *pC-Ste4-S4tc*) and the negative diverter without feedback, or resistance diverter, (*pC-Msg5-S2th*) fail to route cells to the non-mating fate (-/+: 0/20 mM theophylline).

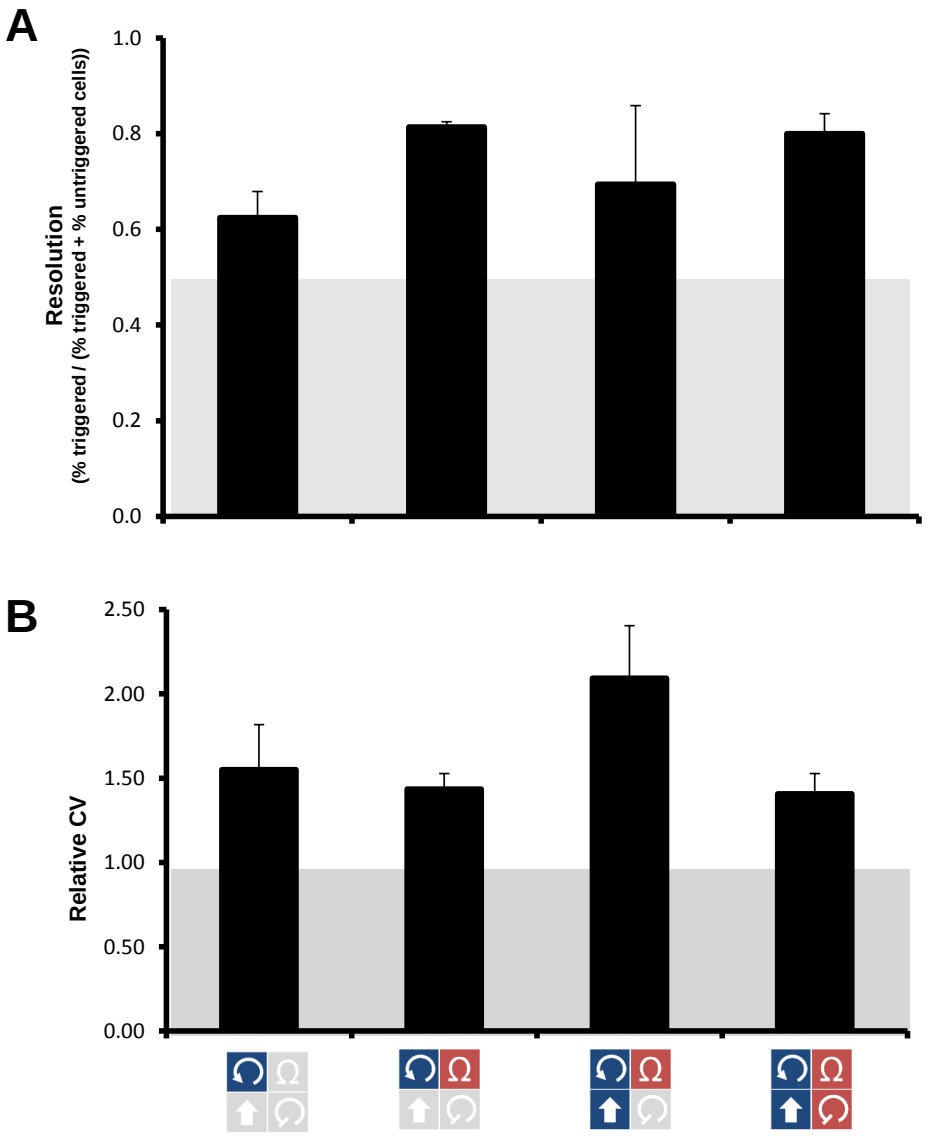

Figure S10. Constructing network architectures for robust performance

(A) Incorporating resistance and negative feedback modules into positive diverter networks enhances resolution between triggered and untriggered cells. Resolution provides a metric for determining the enrichment of triggered cells relative to untriggered cells above a particular fluorescence level, thus providing a measure of certainty that a cell above a particular fluorescence level has been triggered. As resolution increases the fraction of untriggered cells overlapping with the triggered cell population decreases. Resolution was determined by setting a

gate at the lowest ~5% of the triggered population. The percentage of cells in the population falling above this gate were determined for both triggered and untriggered cells (untriggered/triggered: 0/1 mM tetracycline). Resolution is reported as the ratio of the % of triggered cells that fell above this gate to the % of total cells (% triggered + % untriggered) that fell above this gate. No population overlap would result in full resolution (resolution = 1), and for entirely overlapping populations each population would contribute an equivalent percentage of cells resulting in a resolution of 0.5. (B) The introduction of resistance and negative feedback into positive diverters significantly reduces population heterogeneity. The coefficient of variation provides a metric for determining population heterogeneity. The coefficient of variation (CV) was determined for triggered cells (1 mM tetracycline) using the CV function in FlowJo v.10 (Tree Star, Inc.) software package on the population gated viable and above background fluorescence. Values were normalized to the CV for the wild-type pathway stimulated with saturating pheromone (100 nM).

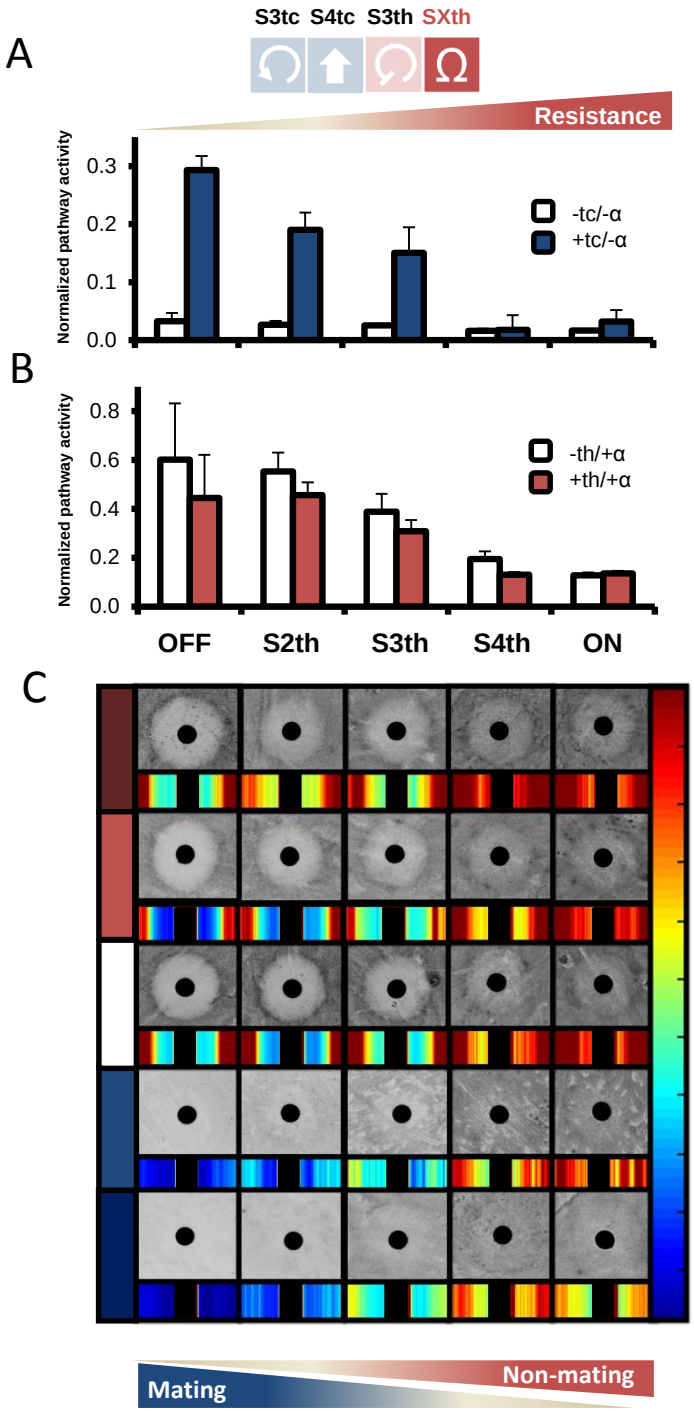

Figure S11. Resistance strength and signal concentration tune activity of diverters to enable dual-fate routing

(A) Pathway activation, (**B**) attenuation, and (**C**) cell fate routing as a function of increasing strength of the resistance module in the dual diverter (–/+tc: 0/1 mM tetracycline; –/+th: 0/5 mM

theophylline; –/+α: 0/100 nM α mating factor). Routing to the non-mating and mating fates is enhanced with increasing levels of the environmental signals (blue: 1 mM tetracycline; dark blue: 2 mM tetracycline; red: 5 mM theophylline; dark red: 20 mM theophylline). Normalized pathway activity from activating constructs is reported as the geometric mean GFP value from cells harboring the specified construct in the absence of pheromone at the indicated signal concentration normalized to that of the control (cells harboring a blank plasmid in the presence of saturating pheromone). Normalized pathway activity from attenuating constructs is reported as the geometric mean GFP value from cells harboring the specified construct in the presence of saturating pheromone at the indicated signal concentration normalized to that of the control (cells harboring a blank plasmid in the presence of saturating pheromone).

A

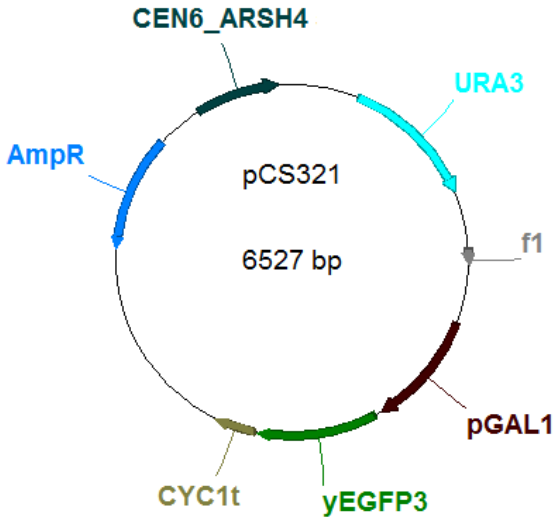

B

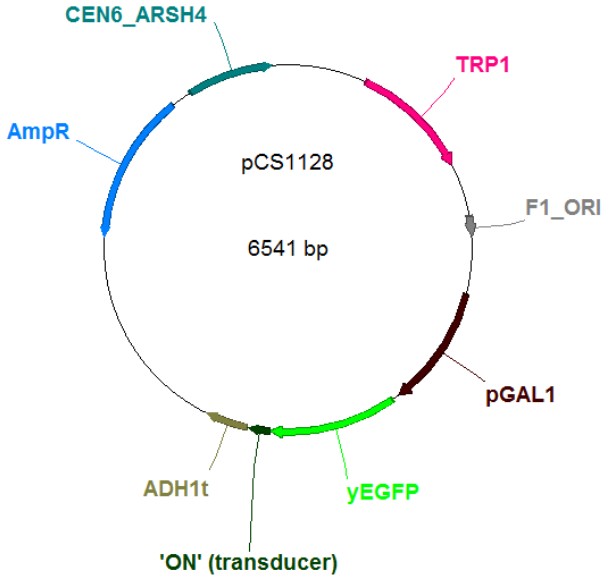

Figure S12. Plasmid maps of single-expression cassette plasmids

Plasmid maps for (A) pCS321 and (B) pCS1128.

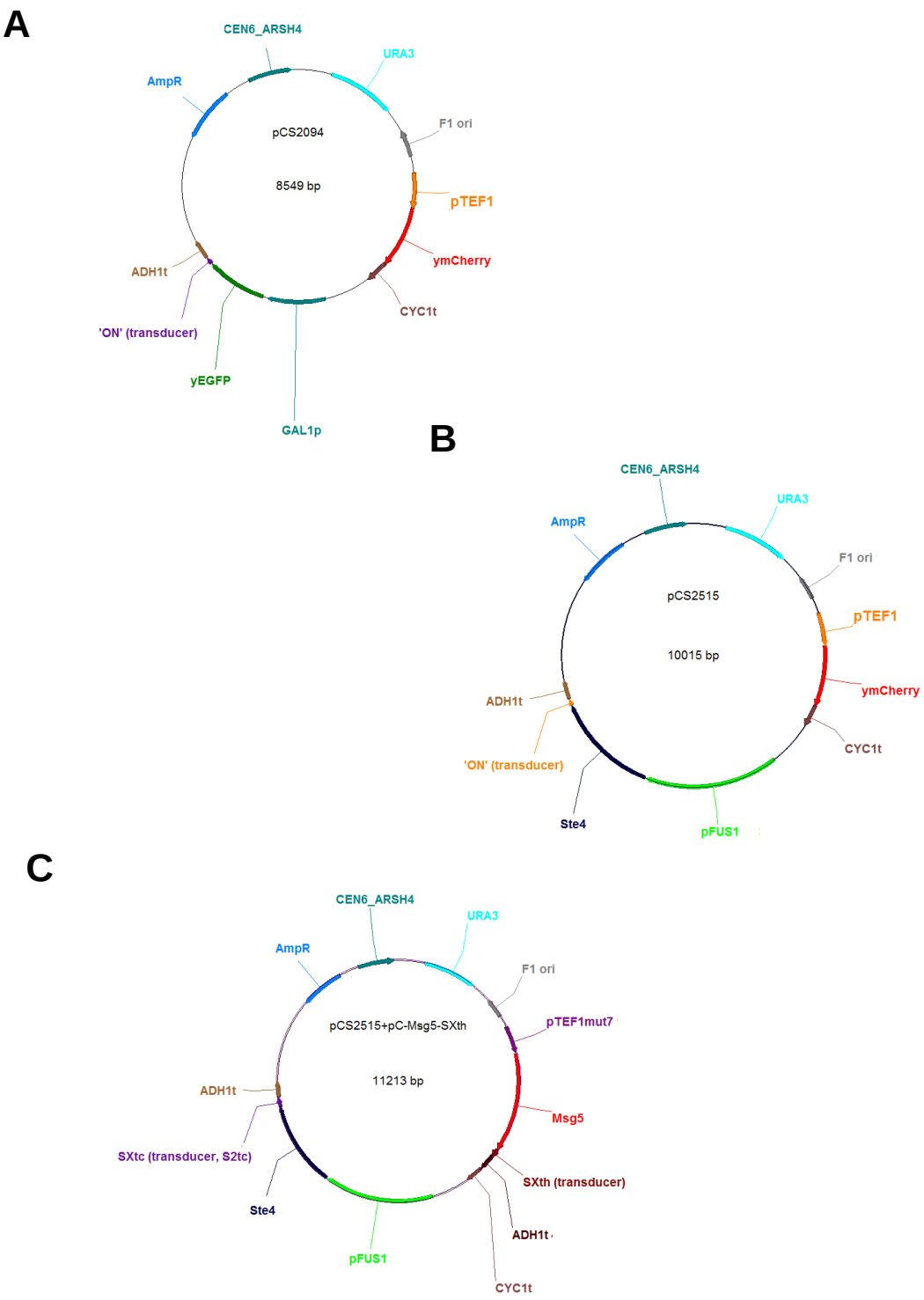

Figure S13. Plasmid maps of -URA dual-expression cassette plasmids

Plasmid maps for (A) pCS2094, (B) pCS2515, and (C) pCS2515 with resistance module (*pC-Msg5-SXth*).

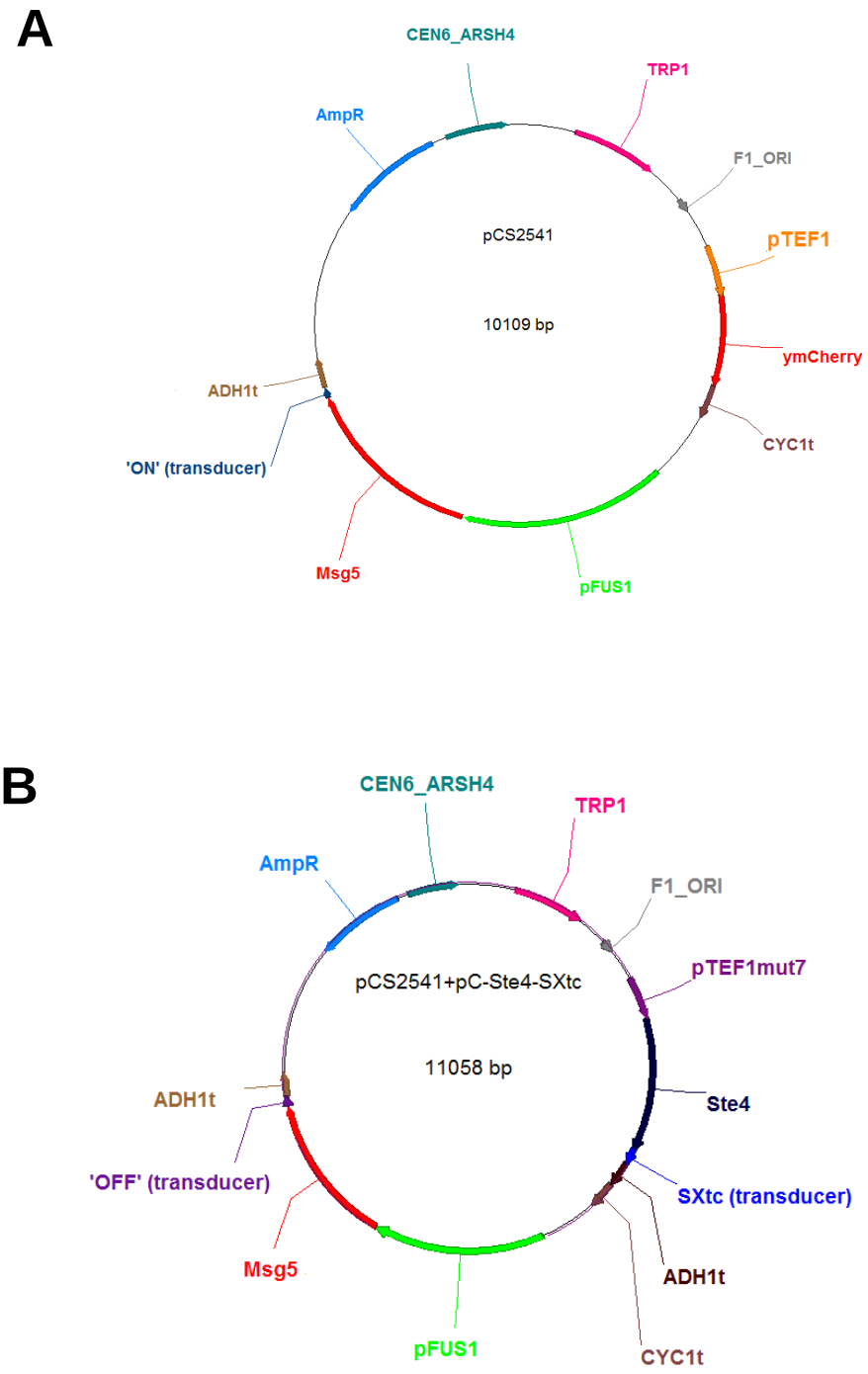

Figure S14. Plasmid maps of –TRP dual-expression cassette plasmids

Plasmid maps for (A) pCS2541 and (B) pCS2541 with booster module (*pC-Ste4-SXtc*).

Supplementary Tables

Table S1. Fitted Hill function and parameters for Ste4

$$\text{pFUS1} - \text{GFP} = Basal + V_{max-Ste4}\frac{[Ste4]^n}{[EC_{50-Ste4}]^n + [Ste4]^n}$$

Parameters	pC-Ste4	pFB-Ste4
n	2.0	1.5
$EC_{50\text{-}Ste4}$	0.21	0.02
Basal	0.07	0.07
$V_{max\text{-}Ste4}$	0.45	0.45

**Basal term represents basal activity of the mating pathway. $V_{max\text{-}Ste4}$ constrained to fit both pC and pFB.*

Table S2. Fitted Hill function and parameters for Msg5

$$\text{pFUS1} - \text{GFP} = Active - V_{max-Msg5}\frac{[Msg5]^n}{[EC_{50-Msg5}]^n + [Msg5]^n}$$

Parameters	pC-Msg5	pFB-Msg5
n	2.3	1.4
$EC_{50\text{-}Msg5}$	0.025	0.024
Active	1.0	1.0
$V_{max\text{-}Msg5}$	0.86	0.53

**Active term represents full activity of the mating pathway at 100 nM pheromone (saturated).*

Table S3. Model Species and Parameters

Species	Description	β (production)	LB	UB
Fus1	Promoter activity, pathway output	0.001	1E-03	2
Fus3	MAPK, central hub in pathway	0.1	1E-03	1
Msg5	Native Msg5, negative regulator	0.01	1E-03	1
Ste4	Native Ste4, positive regulator	0.2	1E-04	0.5

Species	Description	δ (degadation)	LB	UB
Fus1	Promoter activity, pathway output	1	1E-03	3
Fus3	MAPK, central hub in pathway	0.7	1E-03	1
Msg5	Native Msg5, negative regulator	3	1E-03	5
Ste4	Native Ste4, positive regulator	2	1E-03	5

Rates	Description	Value	LB	UB
k_{α}	Rate constant for α-factor activation of Fus3	2	0.50	4
k_{Fus3}	Rate constant for Fus3 activation of Fus1	1.3	1E-03	2
k_{Ste4}	Rate constant for Ste4 activation of Fus3	1	1E-03	5
k_{Msg5}	Rate constant for Msg5 desphosphorylation of Fus3	10	1E-03	15
$k_{c,Ste4}$	Rate constant for production of Ste4 from booster module	2	1E-03	5
$k_{FB,Ste4}$	Rate constant for production of Ste4 from positive feedback module	2	1E-03	5
$k_{c,Msg5}$	Rate constant for production of Msg5 from resistance module	2.5	1E-03	5
$k_{FB,Msg5}$	Rate constant for production of Msg5 from negative feedback module	1.5	1E-03	5

Hill coefficients	Description	Value	LB	UB
n	Hill coefficient for α-factor effect on Fus3	2	1	5
n_{nf}	Hill coefficient for negative feedback loop, Fus1 production of Msg5	1	1	5
n_{pf}	Hill coefficient for positive feedback loop, Fus1 production of Ste4	3	1	5
m	Hill coefficient for Ste4 activation of Fus3	4	1	5
q	Hill coefficient for Msg5 deactivation of Fus3	4	1	5
p	Hill coefficient for Fus3 activation of Fus1	1	1	5

K_M	Description	Value	LB	UB
$K_{M,\alpha}$	Half-maximal concentration of α-factor (pheromone)	14	10	40
$K_{M,Ste4}$	Half-maximal concentration of Ste4	0.5	1E-03	5
$K_{M,Msg5}$	Half-maximal concentration of Msg5	0.05	1E-03	5
$K_{M,Fus3}$	Half-maximal concentration of Fus3	1	1E-03	2
$K_{M,Fus1,nf}$	Half-maximal concentration of Fus1 for negative feedback loop	1	1E-03	5
$K_{M,Fus1,pf}$	Half-maximal concentration of Fus1 for positive feedback loop	0.1	1E-03	5

Synthetic Inputs	Description	Min	Max
SFtc	Tetracycline-transducer activity of positive feedback module	0	1
SCtc	Tetracycline-transducer activity of booster module	0	1
SFth	Theophylline-transducer activity of negative feedback module	0	1
SCth	Theophylline-transducer activity of resistance module	0	1

***LB = Lower bound, UB= Upper bound**

Table S4. yEGFP plasmids

pCS #	Cassette	3'UTR	Marker
pCS1128	pGAL1-yEGFP-ADH1t	sTRSV Ctrl	TRP
pCS321	pGAL1-yEGFP-ADH1t	Empty	URA
pCS1124	pFUS1 -yEGFP-ADH1t	Empty	URA
pCS1585	pTEF1 -yEGFP-ADH1t	Empty	URA
pCS2446	pTEF7 -yEGFP-ADH1t	Empty	URA
pCS2447	pCYC1-yEGFP-ADH1t	Empty	URA
pCS2448	pADH1-yEGFP-ADH1t	Empty	URA
pCS2449	pSTL1-yEGFP-ADH1t	Empty	URA
pCS1748	pTEF1-yEGFP-ADH1t	Empty	URA
pCS2450	pTEF1-yEGFP-L2b12tcNheI-ADH1t	L2b12tc	URA
pCS2451	pTEF1-yEGFP- L2b12tc-L2bOFF1-ADH1t	L2b12tc-L2bOFF1	URA

Table S5. Promoter and gene-specific primers for cloning

Insert or PCR Product	Primer Name	Sequence	Template
pTEF7	pTEF7-FWD	5'- AA GAGCTC ATA GCT TCA AAA TGT CTC TAC TCC TTT TT	pTEF1mut7 (*55*)
	pTEF7-REV	5'- AAA GGATCC AAC TTA GAT TAG ATT GCT ATG CTT TCT TTC C	
pFUS1	pDS71.FUS1-FWD	5'-TTT GCGGCCGC CCA ATC TCA GAG GCT GAG TCT	pDS71 (*56*)
	pDS71.pFUS1-REV	5'-TTT GGATCC TTT GAT TTT CAG AAA CTT GAT GGC	
pADH1	pADH1-FWD	5'- AA GAGCTC AGC TCG ATA TCC TTT TGT TGT TTC C	pCS13
	pADH1-REV	5'- AA GGATCC ATT GTA TGC TTG GTA TAG CTT GAA ATA TTG TG	
pCYC1	pCYC1-FWD	5'- AA GAGCTC CTC GGT ACC CTA TGG CAT GCA TGT	pCS14
	pCYC1-REV	5'- AAA GGATCCACGAATTGATCCGGTAATTTAGTGTGTG	
Ste4	Ste4.k2.FWD	5'- AAA GGATCC A AT TAA TA ATG GCA GCA CAT CAG ATG GAC	pNTI113 (*20*)
	Ste4.REV	5'-AAA CCTAGG CTATTGATAACCTGGAGACCATA	
Ste50	Ste50. k2.FWD	5' - AAA GGATCC A AT TAA TA ATG GAG GAC GGT AAA CAG G	Genomic Ste50
	Ste50.REV	5- AAA CCTAGG TTA GAG TCT TCC ACC GGG G	
Ste11	Ste11.K2.FWD	5'-AAAAAA GGATCC ATTAAATA ATG GAA CAG ACA CAA ACA GCA GAG	pVS1 (*57*)
	Ste11.Stop.REV	5'- AAAA CCTAGG TCA AATTATGTGTGCATCCAGCCATGGA	
Ste7	Ste7.K2.FWD	5'-AAAAAA GGATCC ATTAAATA ATG TTT CAA CGA AAG ACT TTA CAG AGA AGG	pVS10 (*57*)
	Ste7.AvrII.REV	5'- AAAAA CCTAGG TCA ATG GGT TGA TCT TTC CGA T	
Fus3	Fus3.K2.FWD	5'-AAAAAA GGATCC ATTAAATA ATG CCA AAG AGA ATT GTA TAC AAT ATA TCC AG	pVS15 (*57*)
	Fus3.A. STOP.REV	5'-AAAAAA CCTAGG CTA ACTA AAT ATT TCG TTC CAA ATG AGT TTC TTG AGG	
Msg5	MSG5.K2.FWD	5'- AAA GGATCC A AT TAA TA GTGCACATGCAATTTCAC	Genomic Msg5
	Msg5.REV	5'-AAAA CCTAGG TTAAGGAAGAAACATCATCTG	

Table S6. Galactose titration plasmids

pCS #	Cassette	3'UTR	Marker
pCS1625	pGAL1-Ste4-ADH1t	ON	TRP
pCS1483	pGAL1-Ste11-ADH1t	ON	TRP
pCS1484	pGAL1-Ste7-ADH1t	ON	TRP
pCS1485	pGAL1-Fus3-ADH1t	ON	TRP
pCS1486	pGAL1-Msg5-ADH1t	ON	TRP

Table S7. Mutagenesis Primers

Primer Name	Sequence	Purpose
Ste4. XholmutFWD	GTCACTGGTGTGCGATCGAGTCCAGATGG	Remove XhoI in Ste4
Ste4. XholmutREV	CCATCTGGACTCGATCGCACACCAGTGAC	
Fus3-XHOFWD	GGAGAAGATGTTCCCTAGAGTCAACCCGAAAGG	Remove XhoI in Fus3
Fus3-XHOREV	CCTTTCGGGTTGACTCTAGGGAACATCTTCTCC	
Ste7-AvrIIFWD	GTAACTGGAGAGTTTCCACTAGGTGGGCATAACGA	Remove AvrII in Ste7
Ste7-AvrIIREV	TCGTTATGCCCACCTAGTGGAAACTCTCCAGTTAC	
pCS1441.XholmutFWD	ATGCTGGCGGCCGCATCGAGAGATCTAAG	Remove XhoI from disintegrators
pCS1441.XholmutREV	CTTAGATCTCTCGATGCGGCCGCCAGCAT	

Table S8. RNA transducers

Switches	Alias	Sequence	Basal Expression (0 mM)	Induced Expression (th=5 mM; tc= 1 mM)
ON	sTRSV Ctrl	AAACAAACAAAGCTGTCACCGGATGTGCTTTCCGGTACGTGAGGTCCGTGAGGACAGAACAGCAAAAAGAAAAATAAAAACTCGAG	100.0%	100.0%
OFF	sTRSV	AAACAAACAAAGCTGTCACCGGATGTGCTTTCCGGTCTGATGAGTCCGTGAGGACGAAACAGCAAAAAGAAAAATAAAAACTCGAG	1.2%	1.2%
S1th	L2b8-a1	AAACAAACAAAGCTGTCACCGGAATCAAGGTCCGGTCTGATGAGTCCGTTGTCCATACCAGCATCGTCTTGATGCCCTTGGCAGGGACGGGACGGAGGACGAAACAGCAAAAAGAAAAATAAAAACTCGAG	3.0%	8.0%
S2th	L2b8-a1-t41	AAACAAACAAAGCTGTCACCGGAATCAAGGTCCGGTCTGATGAGTCCGTTGCGTATACCAGCATCGTCTTGATGCCCTTGGCAGACGGTAGACGGAGGACGAAACAGCAAAAAGAAAAATAAAAACTCGAG	3.6%	12.7%
S3th	L2b8-t47	AAACAAACAAAGCTGTCACCGGATGTGCTTTCCGGTCTGATGAGTCCGTTGAGTATACCAGCATCGTCTTGATGCCCTTGGCAGACTGTATACGGAGGACGAAACAGCAAAAAGAAAAATAAAAA	6.1%	33.6%
S4th	L2b8	AAACAAACAAAGCTGTCACCGGATGTGCTTTCCGGTCTGATGAGTCCGTTGTCCATACCAGCATCGTCTTGATGCCCTTGGCAGGGACGGGACGGAGGACGAAACAGCAAAAAGAAAAATAAAAACTCGAG	10.8%	36.7%
S5th	L2b1	AAACAAACAAAGCTGTCACCGGATGTGCTTTCCGGTCTGATGAGTCCGTGTCCATACCAGCATCGTCTTGATGCCCTTGGCAGGGACGGGACGAGGACGAAACAGCAAAAAGAAAAATAAAAA	39.8%	75.3%
S1tc	L2b12tc-11	AAACAAACAAAGCTGTCACCGGATGTGCTTTCCGGTCTGATGAGTCCGTTGTTGAAAACATACCAGATTTCGATCTGGAGAGGTGAAGAATTCGACCACCTCATTTCAACGGAGGACGAAACAGCAAAAAGAAAAATAAAAACTCGAG	3.7%	4.8%
S2tc	L2b8tc-a1	AAACAAACAAAGCTGTCACCGGAATCAAGGTCCGGTCTGATGAGTCCGTTGTCCAAAACATACCAGATTTCGATCTGGAGAGGTGAAGAATTCGACCACCTGGACGGGACGGAGGACGAAACAGCAAAAAGAAAAATAAAAACTCGAGCC	3.0%	10.8%
S3tc	L2b12tc-NheI-L2bOFF1	AAACAAACAAAGCTGTCACCGGATGTGCTTTCCGGTCTGATGAGTCCGTTGTCCAAAACATACCAGATTTCGATCTGGAGAGGTGAAGAATTCGACCACCTGGACGGGACGGAGGACGAAACAGCAAAAAGAAAAATAAAAAGCTAGGAAACAAACAAAGCTGTCACCGGATGTGCTTTCCGGTCTGATGAGTCCGTGTTGCTGATACCAGCATCGTCTTGATGCCCTTGGCAGCAGTGGACGAGGACGAAACAGCAAAAAGAAAAATAAAAA	4.2%	21.2%
S4tc	L2b8tc	AAACAAACAAAGCTGTCACCGGATGTGCTTTCCGGTCTGATGAGTCCGTTGTCCAAAACATACCAGATTTCGATCTGGAGAGGTGAAGAATTCGACCACCTGGACGGGACGGAGGACGAAACAGCAAAAAGAAAAATAAAAACTCGAG	8.4%	43.9%

Note: Data for S3tc characterized in this study all other data acquired previously (*24*, *35*).

Table S9. Primers for amplifying RNA transducers

PCR Product	Primer Name	Sequence
Various Switches	Switch-Fwd	5'-GACCTAGGAAACAAACAAAGCTGTCACC
	Switch-REV	5'-GGCTCGAGTTTTTATTTTTCTTTTTGCTGTTTCG
	Switch.NheI.XhoI.REV	5'-TT CTCGAG TTTTTT GCTAGC TTTTTATTTTTCTTTTTGCTGTTTC
	Switch3'sTRSVCtrl.XhoI.REV	5'-AAAACTCGAG TTTTTATTTTTCTTTTTGCTGTTCTG

Table S10. Msg5 plasmids (URA)

pCS321+pX-Msg5-ADH11t		
pCS #	**Promoter**	**3'UTR**
pCS2452	pADH1	Empty
pCS2453	pCYC1	Empty
pCS2454	pTEF7	Empty
pCS2455	pFUS1	Empty
pCS2456	pADH1	ON
pCS2457	pCYC1	ON
pCS2458	pTEF1	ON
pCS321+pFUS1-Msg5-SXth-ADH1t		
pCS #		**3'UTR**
pCS2459		ON
pCS2460		S5th
pCS2461		S4th
pCS2462		S3th
pCS2463		S2th
pCS2464		S1th
pCS2465		OFF
pCS321+pTEF7-Msg5-SXth-ADH1t		
pCS #		**3'UTR**
pCS2466		ON
pCS2467		S5th
pCS2468		S4th
pCS2469		S3th
pCS2470		S2th
pCS2471		S1th
pCS2472		OFF

Table S11. Ste4 plasmids (URA)

pCS321+pX-Ste4-ADH1t		
pCS #	**Promoter**	**3'UTR**
pCS2473	pADH1	Empty
pCS2474	pCYC1	Empty
pCS2475	pFUS1	Empty
pCS2476	pADH1	ON
pCS2477	pCYC1	ON
pCS2478	pTEF1	ON
pCS2094+pFUS1-Ste4-SXtc-ADH1t		
pCS #		**3'UTR**
pCS2479		ON
pCS2480		S4tc
pCS2481		S3tc
pCS2515		S2tc
pCS2483		S1tc
pCS2484		OFF
pCS321+pFUS1-Ste4-SXth-ADH1t		
pCS #		**3'UTR**
pCS2485		ON
pCS2486		S5th
pCS2487		S4th
pCS2488		S2th
pCS2489		S1th
pCS2490		OFF
pCS321+pFUS1-Ste4-SXtc-ADH1t		
pCS #		**3'UTR**
pCS2491		S4tc
pCS2492		S2tc
pCS2493		S1tc
pCS321+pTEF7-Ste4-SXtc-ADH1t		
pCS #		**3'UTR**
pCS2494		**ON**
pCS2495		S4tc
pCS2496		S3tc
pCS2497		S2tc
pCS2498		S1tc
pCS2499		OFF
pCS321+pTEF7-Ste4-SXth-ADH1t		
pCS #		**3'UTR**
pCS2500		S5th
pCS2501		S4th
pCS2502		S2th
pCS2503		S1th
pCS321+pADH1-Ste4-SXth-ADH1t		
pCS #		**3'UTR**
pCS2504		ON
pCS2505		S5th
pCS2506		S4th
pCS2507		S2th
pCS2508		S1th
pCS2509		OFF

Table S12. pCS2094 series dual expression cassette plasmids (URA)

pCS #	Downstream Cassette	Upstream Cassette	Marker
pCS2094	**pTEF1-yEGFP-ON-ADH1t**	**pTEF1-mcherry-CYC1t**	**URA**
pCS2515	**pFUS1-Ste4-S2tc-ADH1t**	**pTEF1-mcherry-CYC1t**	**URA**
pCS2516	pFUS1-Ste4-S2tc-ADH1t	pTEF7-Msg5-OFF-ADH1t	URA
pCS2517	pFUS1-Ste4-S2tc-ADH1t	pTEF7-Msg5-S2th-ADH1t	URA
pCS2518	pFUS1-Ste4-S2tc-ADH1t	pTEF7-Msg5-S3th-ADH1t	URA
pCS2519	pFUS1-Ste4-S2tc-ADH1t	pTEF7-Msg5-S4th-ADH1t	URA
pCS2520	pFUS1-Ste4-S2tc-ADH1t	pTEF7-Msg5-ON-ADH1t	URA
pCS2521	**pFUS1-Ste4-OFF-ADH1t**	**pTEF1-mcherry-CYC1t**	**URA**
pCS2522	pFUS1-Ste4-OFF-ADH1t	pTEF7-Msg5-S2th-ADH1t	URA
pCS2523	pFUS1-Ste4-OFF-ADH1t	pTEF7-Msg5-S3th-ADH1t	URA
pCS2524	pFUS1-Ste4-OFF-ADH1t	pTEF7-Msg5-S4th-ADH1t	URA
pCS2525	pFUS1-Ste4-OFF-ADH1t	pTEF7-Msg5-ON-ADH1t	URA
pCS2526	**pFUS1-Ste4-S3tc-ADH1t**	**pTEF1-mcherry-CYC1t**	**URA**
pCS2527	pFUS1-Ste4-S3tc-ADH1t	pTEF7-Msg5-OFF-ADH1t	URA
pCS2528	pFUS1-Ste4-S3tc-ADH1t	pTEF7-Msg5-S2th-ADH1t	URA
pCS2529	pFUS1-Ste4-S3tc-ADH1t	pTEF7-Msg5-S3th-ADH1t	URA
pCS2530	pFUS1-Ste4-S3tc-ADH1t	pTEF7-Msg5-S4th-ADH1t	URA
pCS2531	pFUS1-Ste4-S3tc-ADH1t	pTEF7-Msg5-ON-ADH1t	URA
pCS2532	**pFUS1-Ste4-S4tc-ADH1t**	**pTEF1-mcherry-CYC1t**	**URA**
pCS2533	pFUS1-Ste4-S4tc-ADH1t	pTEF7-Msg5-OFF-ADH1t	URA
pCS2534	pFUS1-Ste4-S4tc-ADH1t	pTEF7-Msg5-S2th-ADH1t	URA
pCS2535	pFUS1-Ste4-S4tc-ADH1t	pTEF7-Msg5-S3th-ADH1t	URA
pCS2536	pFUS1-Ste4-S4tc-ADH1t	pTEF7-Msg5-S4th-ADH1t	URA
pCS2537	pFUS1-Ste4-S4tc-ADH1t	pTEF7-Msg5-ON-ADH1t	URA
pCS2538	**pFUS1-Ste4-ON-ADH1t**	**pTEF1-mcherry-CYC1t**	**URA**
pCS2539	pFUS1-Ste4-ON-ADH1t	pTEF7-Msg5-OFF-ADH1t	URA

Table S13. pCS1128 series dual expression cassette plasmids (TRP)

pCS #	Downstream Cassette	Upstream Cassette	Marker
pCS1128	**None**	**pGAL1-yEGFP-ON-ADH1t**	**TRP**
pCS2540	**pFUS1-Ste4-OFF-ADH1t**	**pTEF1-mcherry-CYC1t**	**TRP**
pCS2541	**pFUS1-Msg5-OFF-ADH1t**	**pTEF1-mcherry-CYC1t**	**TRP**
pCS2542	pFUS1-Msg5-OFF-ADH1t	pTEF7-Ste4-S2tc-ADH1t	TRP
pCS2543	pFUS1-Msg5-OFF-ADH1t	pTEF7-Ste4-S3tc-ADH1t	TRP
pCS2544	pFUS1-Msg5-OFF-ADH1t	pTEF7-Ste4-S4tc-ADH1t	TRP
pCS2545	pFUS1-Msg5-OFF-ADH1t	pTEF7-Ste4-ON-ADH1t	TRP
pCS2546	**pFUS1-Msg5-S2th-ADH1t**	**pTEF1-mcherry-CYC1t**	**TRP**
pCS2547	pFUS1-Msg5-S2th-ADH1t	pTEF7-Ste4-OFF-ADH1t	TRP
pCS2548	pFUS1-Msg5-S2th-ADH1t	pTEF7-Ste4-S2tc-ADH1t	TRP
pCS2549	pFUS1-Msg5-S2th-ADH1t	pTEF7-Ste4-S3tc-ADH1t	TRP
pCS2550	pFUS1-Msg5-S2th-ADH1t	pTEF7-Ste4-S4tc-ADH1t	TRP
pCS2551	pFUS1-Msg5-S2th-ADH1t	pTEF7-Ste4-ON-ADH1t	TRP
pCS2552	**pFUS1-Msg5-S3th-ADH1t**	**pTEF1-mcherry-CYC1t**	**TRP**
pCS2553	pFUS1-Msg5-S3th-ADH1t	pTEF7-Ste4-OFF-ADH1t	TRP
pCS2554	pFUS1-Msg5-S3th-ADH1t	pTEF7-Ste4-S2tc-ADH1t	TRP
pCS2555	pFUS1-Msg5-S3th-ADH1t	pTEF7-Ste4-S3tc-ADH1t	TRP
pCS2556	pFUS1-Msg5-S3th-ADH1t	pTEF7-Ste4-S4tc-ADH1t	TRP
pCS2557	pFUS1-Msg5-S3th-ADH1t	pTEF7-Ste4-ON-ADH1t	TRP
pCS2558	**pFUS1-Msg5-S4th-ADH1t**	**pTEF1-mcherry-CYC1t**	**TRP**
pCS2559	pFUS1-Msg5-S4th-ADH1t	pTEF7-Ste4-OFF-ADH1t	TRP
pCS2560	pFUS1-Msg5-S4th-ADH1t	pTEF7-Ste4-S2tc-ADH1t	TRP
pCS2561	pFUS1-Msg5-S4th-ADH1t	pTEF7-Ste4-S3tc-ADH1t	TRP
pCS2562	pFUS1-Msg5-S4th-ADH1t	pTEF7-Ste4-S4tc-ADH1t	TRP
pCS2563	pFUS1-Msg5-S4th-ADH1t	pTEF7-Ste4-ON-ADH1t	TRP
pCS2564	**pFUS1-Msg5-ON-ADH1t**	**pTEF1-mcherry-CYC1t**	**TRP**
pCS2565	pFUS1-Msg5-ON-ADH1t	pTEF7-Ste4-OFF-ADH1t	TRP
pCS2566	pFUS1-Msg5-ON-ADH1t	pTEF7-Ste4-S2tc-ADH1t	TRP
pCS2567	pFUS1-Msg5-ON-ADH1t	pTEF7-Ste4-S3tc-ADH1t	TRP

Table S14. Ste4 plasmids (TRP)

pCS1128+pTEF7-Ste4-SXtc-ADH1t	
pCS #	**3'UTR**
pCS2510	S4tc
pCS2511	S3tc
pCS2512	S2tc
pCS2513	S1tc
pCS2514	OFF

Table S15. Integration plasmids

pCS #	Cassette	ntegration Loc	Marker
pCS1391	LoxP Integrating plasmid (*58*)	Primer-specific	G418
pCS2292	pCS1391+pFUS1-yEGFP-ADH1t	Primer-specific	G418

Table S16. Yeast strains

CSY#	Description
CSY364	EY1119 from (*59*); W303a ∆sst1 ∆kss1::HIS3
CSY408	CSY364 Δgal2::KanR
CSY505	CSY364 LYS2::pFUS1-GFP-ADH1t
CSY532	CSY364 Δgal2::pFUS1-GFP-ADH1t-loxP-KanR-loxP
CSY840	CSY364 Δtrp1::pFUS1-yEGFP3-ADH1t-loxP-KanR-loxP

Table S17. Integrating Primers

Loci	Sequence	Direction
GAL2	ATGCACCTTATTCAATTATCATCAAGAATAGTAATAGTTAAGTAAACACAA GATTAACATAGATTGTACTGAGAGTGCAC	FWD
	ATGATAATTAAAATGAAGAAAAAACGTCAGTCATGAAAAATTAAGAGAG ATGATGGAGCGCGACTCACTATAGGGAGACC	REV
TRP	GTATACGTGATTAAGCACACAAAGGCAGCTTGGAGTATGTCTGTTATTAA TTTCACAGGAAGATTGTACTGAGAGTGCAC	FWD
	TTGCTTTTCAAAAGGCCTGCAGGCAAGTGCACAAACAATACTTAAATAAA TACTACTCAGCGACTCACTATAGGGAGACC	REV

References and Notes

1. R. Seger, E. G. Krebs, The MAPK signaling cascade. *FASEB J.* **9**, 726–735 (1995). Medline

2. K. L. Pierce, R. T. Premont, R. J. Lefkowitz, Seven-transmembrane receptors. *Nat. Rev. Mol. Cell Biol.* **3**, 639–650 (2002). doi:10.1038/nrm908 Medline

3. A. Negro, B. K. Brar, K. F. Lee, Essential roles of Her2/erbB2 in cardiac development and function. *Recent Prog. Horm. Res.* **59**, 1–12 (2004). doi:10.1210/rp.59.1.1 Medline

4. Y. Y. Chen, M. C. Jensen, C. D. Smolke, Genetic control of mammalian T-cell proliferation with synthetic RNA regulatory systems. *Proc. Natl. Acad. Sci. U.S.A.* **107**, 8531–8536 (2010). doi:10.1073/pnas.1001721107 Medline

5. S. J. Culler, K. G. Hoff, C. D. Smolke, Reprogramming cellular behavior with RNA controllers responsive to endogenous proteins. *Science* **330**, 1251–1255 (2010). doi:10.1126/science.1192128 Medline

6. J. C. Anderson, E. J. Clarke, A. P. Arkin, C. A. Voigt, Environmentally controlled invasion of cancer cells by engineered bacteria. *J. Mol. Biol.* **355**, 619–627 (2006). doi:10.1016/j.jmb.2005.10.076 Medline

7. C. Kemmer, M. Gitzinger, M. Daoud-El Baba, V. Djonov, J. Stelling, M. Fussenegger, Self-sufficient control of urate homeostasis in mice by a synthetic circuit. *Nat. Biotechnol.* **28**, 355–360 (2010). doi:10.1038/nbt.1617 Medline

8. W. Weber, M. Daoud-El Baba, M. Fussenegger, Synthetic ecosystems based on airborne inter- and intrakingdom communication. *Proc. Natl. Acad. Sci. U.S.A.* **104**, 10435–10440 (2007). doi:10.1073/pnas.0701382104 Medline

9. H. Ye, M. Daoud-El Baba, R. W. Peng, M. Fussenegger, A synthetic optogenetic transcription device enhances blood-glucose homeostasis in mice. *Science* **332**, 1565–1568 (2011). doi:10.1126/science.1203535 Medline

10. Z. Xie, L. Wroblewska, L. Prochazka, R. Weiss, Y. Benenson, Multi-input RNAi-based logic circuit for identification of specific cancer cells. *Science* **333**, 1307–1311 (2011). doi:10.1126/science.1205527 Medline

11. J. M. Callura, D. J. Dwyer, F. J. Isaacs, C. R. Cantor, J. J. Collins, Tracking, tuning, and terminating microbial physiology using synthetic riboregulators. *Proc. Natl. Acad. Sci. U.S.A.* **107**, 15898–15903 (2010). doi:10.1073/pnas.1009747107 Medline

12. T. L. Deans, C. R. Cantor, J. J. Collins, A tunable genetic switch based on RNAi and repressor proteins for regulating gene expression in mammalian cells. *Cell* **130**, 363–372 (2007). doi:10.1016/j.cell.2007.05.045 Medline

13. H. Kobayashi, M. Kaern, M. Araki, K. Chung, T. S. Gardner, C. R. Cantor, J. J. Collins, Programmable cells: interfacing natural and engineered gene networks. *Proc. Natl. Acad. Sci. U.S.A.* **101**, 8414–8419 (2004). doi:10.1073/pnas.0402940101 Medline

14. Y. Y. Chen, K. E. Galloway, C. D. Smolke, Synthetic biology: advancing biological frontiers by building synthetic systems. *Genome Biol.* **13**, 240 (2012). doi:10.1186/gb-2012-13-2-240 Medline

15. D. Hanahan, R. A. Weinberg, The hallmarks of cancer. *Cell* **100**, 57–70 (2000). doi:10.1016/S0092-8674(00)81683-9 Medline

16. F. McCormick, Signalling networks that cause cancer. *Trends Cell Biol.* **9**, M53–M56 (1999). doi:10.1016/S0962-8924(99)01668-2 Medline

17. H. G. Dohlman, J. W. Thorner, Regulation of G protein-initiated signal transduction in yeast: paradigms and principles. *Annu. Rev. Biochem.* **70**, 703–754 (2001). doi:10.1146/annurev.biochem.70.1.703 Medline

18. E. A. Elion, Pheromone response, mating and cell biology. *Curr. Opin. Microbiol.* **3**, 573–581 (2000). doi:10.1016/S1369-5274(00)00143-0 Medline

19. C. J. Bashor, N. C. Helman, S. Yan, W. A. Lim, Using engineered scaffold interactions to reshape MAP kinase pathway signaling dynamics. *Science* **319**, 1539–1543 (2008). doi:10.1126/science.1151153 Medline

20. N. T. Ingolia, A. W. Murray, Positive-feedback loops as a flexible biological module. *Curr. Biol.* **17**, 668–677 (2007). doi:10.1016/j.cub.2007.03.016 Medline

21. S. H. Park, A. Zarrinpar, W. A. Lim, Rewiring MAP kinase pathways using alternative scaffold assembly mechanisms. *Science* **299**, 1061–1064 (2003). doi:10.1126/science.1076979 Medline

22. S. D. Santos, P. J. Verveer, P. I. Bastiaens, Growth factor-induced MAPK network topology shapes Erk response determining PC-12 cell fate. *Nat. Cell Biol.* **9**, 324–330 (2007). doi:10.1038/ncb1543 Medline

23. E. Franco, F. Blanchini, Structural properties of the MAPK pathway topologies in PC12 cells. *J. Math. Biol.* (2012). doi:10.1007/s00285-012-0606-x

24. M. N. Win, C. D. Smolke, A modular and extensible RNA-based gene-regulatory platform for engineering cellular function. *Proc. Natl. Acad. Sci. U.S.A.* **104**, 14283–14288 (2007). doi:10.1073/pnas.0703961104 Medline

25. R. G. Palpant, R. Steimnitz, T. H. Bornemann, K. Hawkins, The Carter Center Mental Health Program: addressing the public health crisis in the field of mental health through policy change and stigma reduction. *Prev. Chronic Dis.* **3**, A62 (2006). Medline

26. M. Osterberg, H. Kim, J. Warringer, K. Melén, A. Blomberg, G. von Heijne, Phenotypic effects of membrane protein overexpression in Saccharomyces cerevisiae. *Proc. Natl. Acad. Sci. U.S.A.* **103**, 11148–11153 (2006). doi:10.1073/pnas.0604078103 Medline

27. S. A. Chapman, A. R. Asthagiri, Quantitative effect of scaffold abundance on signal propagation. *Mol. Syst. Biol.* **5**, 313 (2009). doi:10.1038/msb.2009.73 Medline

28. H. B. Fraser, A. E. Hirsh, G. Giaever, J. Kumm, M. B. Eisen, Noise minimization in eukaryotic gene expression. *PLoS Biol.* **2**, e137 (2004). doi:10.1371/journal.pbio.0020137 Medline

29. J. Stelling, E. D. Gilles, F. J. Doyle, 3rd, Robustness properties of circadian clock architectures. *Proc. Natl. Acad. Sci. U.S.A.* **101**, 13210–13215 (2004). doi:10.1073/pnas.0401463101 Medline

30. J. Stelling, U. Sauer, Z. Szallasi, F. J. Doyle, 3rd, J. Doyle, Robustness of cellular functions. *Cell* **118**, 675–685 (2004). doi:10.1016/j.cell.2004.09.008 Medline

31. A. Eldar, R. Dorfman, D. Weiss, H. Ashe, B. Z. Shilo, N. Barkai, Robustness of the BMP morphogen gradient in Drosophila embryonic patterning. *Nature* **419**, 304–308 (2002). doi:10.1038/nature01061 Medline

32. G. Stoll, M. Bischofberger, J. Rougemont, F. Naef, Stabilizing patterning in the Drosophila segment polarity network by selecting models in silico. *Biosystems* **102**, 3–10 (2010). doi:10.1016/j.biosystems.2010.07.014 Medline

33. E. C. O'Shaughnessy, S. Palani, J. J. Collins, C. A. Sarkar, Tunable signal processing in synthetic MAP kinase cascades. *Cell* **144**, 119–131 (2011). doi:10.1016/j.cell.2010.12.014 Medline

34. T. M. Thomson, K. R. Benjamin, A. Bush, T. Love, D. Pincus, O. Resnekov, R. C. Yu, A. Gordon, A. Colman-Lerner, D. Endy, R. Brent, Scaffold number in yeast signaling system sets tradeoff between system output and dynamic range. *Proc. Natl. Acad. Sci. U.S.A.* **108**, 20265–20270 (2011). doi:10.1073/pnas.1004042108 Medline

35. J. C. Liang, A. L. Chang, A. B. Kennedy, C. D. Smolke, A high-throughput, quantitative cell-based screen for efficient tailoring of RNA device activity. *Nucleic Acids Res.* **40**, e154 (2012). doi:10.1093/nar/gks636 Medline

36. A. Becskei, L. Serrano, Engineering stability in gene networks by autoregulation. *Nature* **405**, 590–593 (2000). doi:10.1038/35014651 Medline

37. C. L. Beisel, C. D. Smolke, Design principles for riboswitch function. *PLOS Comput. Biol.* **5**, e1000363 (2009). doi:10.1371/journal.pcbi.1000363 Medline

38. C. J. Marshall, Specificity of receptor tyrosine kinase signaling: transient versus sustained extracellular signal-regulated kinase activation. *Cell* **80**, 179–185 (1995). doi:10.1016/0092-8674(95)90401-8 Medline

39. C. Banerjee, A. Javed, J. Y. Choi, J. Green, V. Rosen, A. J. van Wijnen, J. L. Stein, J. B. Lian, G. S. Stein, Differential regulation of the two principal Runx2/Cbfa1 n-terminal isoforms in response to bone morphogenetic protein-2 during development of the osteoblast phenotype. *Endocrinology* **142**, 4026–4039 (2001). doi:10.1210/en.142.9.4026 Medline

40. Y. Yuan, J. D. Chung, X. Fu, V. E. Johnson, P. Ranjan, S. L. Booth, S. A. Harding, C. J. Tsai, Alternative splicing and gene duplication differentially shaped the regulation of isochorismate synthase in Populus and Arabidopsis. *Proc. Natl.*

Acad. Sci. U.S.A. **106**, 22020–22025 (2009). doi:10.1073/pnas.0906869106 Medline

41. U. S. Bhalla, P. T. Ram, R. Iyengar, MAP kinase phosphatase as a locus of flexibility in a mitogen-activated protein kinase signaling network. *Science* **297**, 1018–1023 (2002). doi:10.1126/science.1068873 Medline

42. W. Wu, T. Pew, M. Zou, D. Pang, S. D. Conzen, Glucocorticoid receptor-induced MAPK phosphatase-1 (MPK-1) expression inhibits paclitaxel-associated MAPK activation and contributes to breast cancer cell survival. *J. Biol. Chem.* **280**, 4117–4124 (2005). doi:10.1074/jbc.M411200200 Medline

43. W. Wu, S. Chaudhuri, D. R. Brickley, D. Pang, T. Karrison, S. D. Conzen, Microarray analysis reveals glucocorticoid-regulated survival genes that are associated with inhibition of apoptosis in breast epithelial cells. *Cancer Res.* **64**, 1757–1764 (2004). doi:10.1158/0008-5472.CAN-03-2546 Medline

44. S. Srikanth, C. C. Franklin, R. C. Duke, R. S. Kraft, Human DU145 prostate cancer cells overexpressing mitogen-activated protein kinase phosphatase-1 are resistant to Fas ligand-induced mitochondrial perturbations and cellular apoptosis. *Mol. Cell. Biochem.* **199**, 169–178 (1999). doi:10.1023/A:1006980326855 Medline

45. J. Y. Wang, C. H. Lin, C. H. Yang, T. H. Tan, Y. R. Chen, Biochemical and biological characterization of a neuroendocrine-associated phosphatase. *J. Neurochem.* **98**, 89–101 (2006). doi:10.1111/j.1471-4159.2006.03852.x Medline

46. G. F. Sprague, Jr., Assay of yeast mating reaction. *Methods Enzymol.* **194**, 77–93 (1991). doi:10.1016/0076-6879(91)94008-Z Medline

47. C. Y. Huang, J. E. Ferrell, Jr., Ultrasensitivity in the mitogen-activated protein kinase cascade. *Proc. Natl. Acad. Sci. U.S.A.* **93**, 10078–10083 (1996). doi:10.1073/pnas.93.19.10078 Medline

48. D. Angeli, J. E. Ferrell, Jr., E. D. Sontag, Detection of multistability, bifurcations, and hysteresis in a large class of biological positive-feedback systems. *Proc. Natl. Acad. Sci. U.S.A.* **101**, 1822–1827 (2004). doi:10.1073/pnas.0308265100 Medline

49. W. Kolch, M. Calder, D. Gilbert, When kinases meet mathematics: the systems biology of MAPK signalling. *FEBS Lett.* **579**, 1891–1895 (2005). doi:10.1016/j.febslet.2005.02.002 Medline

50. X. L. Zhan, R. J. Deschenes, K. L. Guan, Differential regulation of FUS3 MAP kinase by tyrosine-specific phosphatases PTP2/PTP3 and dual-specificity phosphatase MSG5 in Saccharomyces cerevisiae. *Genes Dev.* **11**, 1690–1702 (1997). doi:10.1101/gad.11.13.1690 Medline

51. J. Andersson, D. M. Simpson, M. Qi, Y. Wang, E. A. Elion, Differential input by Ste5 scaffold and Msg5 phosphatase route a MAPK cascade to multiple outcomes. *EMBO J.* **23**, 2564–2576 (2004). doi:10.1038/sj.emboj.7600250 Medline

52. B. Kofahl, E. Klipp, Modelling the dynamics of the yeast pheromone pathway. *Yeast* **21**, 831–850 (2004). doi:10.1002/yea.1122 Medline

53. J. Sambrook, E. F. Fritsch, T. Maniatis, *Molecular Cloning: A Laboratory Manual, Third edition* (Cold Spring Harbor Lab Press, Cold Spring Harbor, NY, 2001).

54. C. Guthrie, G. Fink, *Guide to Yeast Genetics and Molecular and Cell Biology*. J. N. Abelson, M. I. Simon, Eds. (Elsevier, London, 2004), vol. 194, pp. 79–92.

55. E. Nevoigt, J. Kohnke, C. R. Fischer, H. Alper, U. Stahl, G. Stephanopoulos, Engineering of promoter replacement cassettes for fine-tuning of gene expression in Saccharomyces cerevisiae. *Appl. Environ. Microbiol.* **72**, 5266–5273 (2006). doi:10.1128/AEM.00530-06 Medline

56. D. E. Siekhaus, D. G. Drubin, Spontaneous receptor-independent heterotrimeric G-protein signalling in an RGS mutant. *Nat. Cell Biol.* **5**, 231–235 (2003). doi:10.1038/ncb941 Medline

57. F. van Drogen, V. M. Stucke, G. Jorritsma, M. Peter, MAP kinase dynamics in response to pheromones in budding yeast. *Nat. Cell Biol.* **3**, 1051–1059 (2001). doi:10.1038/ncb1201-1051 Medline

58. U. Güldener, S. Heck, T. Fielder, J. Beinhauer, J. H. Hegemann, A new efficient gene disruption cassette for repeated use in budding yeast. *Nucleic Acids Res.* **24**, 2519–2524 (1996). doi:10.1093/nar/24.13.2519 Medline

59. A. Flotho, D. M. Simpson, M. Qi, E. A. Elion, Localized feedback phosphorylation of Ste5p scaffold by associated MAPK cascade. *J. Biol. Chem.* **279**, 47391–47401 (2004). doi:10.1074/jbc.M405681200 Medline

60. A. P. Won, J. E. Garbarino, W. A. Lim, Recruitment interactions can override catalytic interactions in determining the functional identity of a protein kinase. *Proc. Natl. Acad. Sci. U.S.A.* **108**, 9809–9814 (2011). doi:10.1073/pnas.1016337108 Medline